Multiple Rayleigh Scattering of Electromagnetic Waves

E. Amic, J. Luck, Th. Nieuwenhuizen

J. Phys. I France 7 (1997) 445–483 MARCH 1997, PAGE 445

Multiple Rayleigh Scattering of Electromagnetic Waves

E. Amic ([1]), J.M. Luck ([1,*]) and Th.M. Nieuwenhuizen ([2])

([1]) CEA Saclay, Service de Physique Théorique, 91191 Gif-sur-Yvette Cedex, France
([2]) Van der Waals-Zeeman Laboratorium, Valckenierstraat 65,
1018 XE Amsterdam, The Netherlands

(Received 22 August 1996, received in final form 7 November 1996, accepted 19 November 1996)

PACS.42.68.Ay – Propagation, transmission, attenuation, and radiative transfer
PACS.42.25.Bs – Wave propagation, transmission and absorption
PACS.42.68.Mj – Scattering, polarization

Abstract. — Multiple scattering of polarized electromagnetic waves in diffusive media is investigated by means of radiative transfer theory. This approach amounts to summing the ladder diagrams for the diffuse reflected or transmitted intensity, or the cyclical ones for the cone of enhanced backscattering. The method becomes exact in several situations of interest, such as a thick-slab experiment (slab thickness $L \gg$ mean free path $\ell \gg$ wavelength λ). The present study is restricted to Rayleigh scattering. It incorporates in a natural way the dependence on the incident and detected polarizations, and takes full account of the internal reflections at the boundaries of the sample, due to the possible mismatch between the mean optical index n of the medium and that n_1 of the surroundings. This work does not rely on the diffusion approximation. It therefore correctly describes radiation in the skin layers, where a crossover takes place between free and diffusive propagation, and *vice-versa*. Quantities of interest, such as the polarization-dependent, angle-resolved mean diffuse intensity in reflection and in transmission, and the shape of the cone of enhanced backscattering, are predicted in terms of solutions to Schwarzschild-Milne equations. The latter are obtained analytically, both in the absence of internal reflections ($n = n_1$), and in the regime of a large index mismatch ($n/n_1 \ll 1$ or $\gg 1$).

1. Introduction

Light undergoes multiple scattering when propagating through inhomogeneous media over distances much larger than one mean free path ℓ. This may occur in a wide variety of situations, ranging from the atmospheres of stars and planets to biological tissues. The theory of multiple scattering of electromagnetic waves is an old classical area of physics [1–4], which has been developed for almost one century, mostly by astrophysicists. This subject has been experiencing an important revival of theoretical and experimental activity for one decade, motivated by the analogy between the effects of random disorder (weak or strong localization) on the propagation of classical waves (electromagnetic, acoustic, seismic) and of quantum-mechanical waves (electrons in solids). The first weak-localization effect to be discovered has been the celebrated enhanced backscattering phenomenon, which takes place in a narrow angular cone around the direction of exact backscattering [5].

(*) Author for correspondence (e-mail: luck@spht.saclay.cea.fr)

Typical laboratory experiments on multiple light scattering involve suspensions of polystyrene spheres or of TiO_2 (white paint) grains in fluids. In these situations the mean free path ℓ is usually much larger than the wavelength λ of light, and the samples are often optically thick slabs, of thickness $L \gg \ell$. The regime of interest, *i.e.*, $\lambda \ll \ell \ll L$, is characterized by a diffusive transport of radiation through multiple scattering. This diffusive regime admits three different levels of theoretical description. (i) The crudest approach is the diffusion approximation, where the multiply scattered intensity is described by means of an effective diffusion equation. The latter is only valid on length scales larger than ℓ, so that is has to be supplemented by boundary conditions. As a consequence, this approach somehow keeps a phenomenological character. (ii) The mesoscopic approach, known as radiative transfer theory (RTT), has been used for long by the community of astrophysicists [1–4]. It is based on a local balance equation, keeping track of the direction of propagation of the intensity. (iii) The systematic microscopic approach consists in expanding the solution of the Maxwell equations in the random medium as a diagrammatic Born (multiple-scattering) series.

In multiple light scattering experiments the quantities of most interest are the mean diffuse reflected and transmitted intensity, and the shape of the peak of enhanced backscattering. For these observables the diagrammatic approach greatly simplifies in the regime $\lambda \ll \ell \ll L$. As far as mean quantities, averaged over the random positions of the scatterers, are concerned, the diffuse radiation is described by the sum of the ladder diagrams, which, in turn, amounts to RTT; the enhanced backscattering phenomenon is described by the so-called cyclical or maximally-crossed diagrams, which can also be summed up by an adaptation of RTT [6,7]. On the other hand, the validity of vector RTT has been established on a rigorous basis [8], starting from a perturbative treatment of Maxwell's equations, extending earlier developments [9] on multiple scattering of electromagnetic waves in plasmas. In the regime where the random fluctuations of the dielectric constant have short-range correlations, this approach rigorously justifies the use of the Schwarzschild-Milne equation of vector RTT with the Rayleigh phase function, which will be the purpose of the present work.

The principles of vector RTT for electromagnetic waves, taking into account their polarizations, are exposed in the book by Chandrasekhar [1], which also contains a formal analytical derivation of the diffuse intensity for Rayleigh scattering, in the absence of internal reflections. This approach is needed in order to obtain predictions at a quantitative level, concerning observables like the diffuse intensity in reflection and in transmission, and the enhanced backscattering cone. In particular the diffusion approximation alone cannot yield such accurate predictions, chiefly because boundary conditions cannot be dealt with in a fully satisfactory way. Surprisingly enough, in the modern era of multiple scattering only very few authors have used RTT. Thus far the major investigations of the weak localization of light, including polarization effects, have rather used either the diffusion approximation [10–12] or numerical simulations [13]. Several other bulk properties of multiple scattering of electromagnetic waves have been investigated along these lines, including especially the effects of Faraday rotation [12,14,15] and of absorption [16]. Exact results on polarization effects on the backscattering cone have only appeared very recently. Mishchenko [17] has derived general properties of the behaviour of polarizations under time reversal, obtaining thus for the first time a consistent derivation of the enhancement factors in the direction of exact backscattering. The full shape of the backscattering cone has then been investigated by Ozrin [18], who did not, however, come up with a full analytical solution of the latter problem. In previous works, we have considered the case of scalar waves undergoing multiple isotropic [19, 20] and arbitrary anisotropic scattering [21]. We have shown how RTT takes proper account of the skin layers, where light is converted over a few mean free paths from a free beam to a diffusive field and *vice-versa*, and how it allows to deal with the effects of internal reflections due to the index

Table I. — *Definitions and notations for kinematic and other useful quantities.*

	outside medium	inside medium
optical index	n_1	$n = mn_1$
wavenumber	$k_1 = n_1\omega/c = 2\pi/\lambda_1$	$k = n\omega/c = 2\pi/\lambda$
incidence angle	θ_1 $\cos\theta_1 = \sqrt{1 - m^2\nu^2}$ $\sin\theta_1 = m\nu$	θ $\cos\theta = \mu$ $\sin\theta = \nu = \sqrt{1-\mu^2}$
parallel wavevector	$p = k_1 \cos\theta_1$	$P = k\cos\theta$
total reflection condition	$m < 1$ and $\sin\theta_1 > m$ (*i.e.* P imaginary)	$m > 1$ and $\sin\theta > 1/m$ (*i.e.* p imaginary)
transverse wavevector	$\lvert\mathbf{q}\rvert = q = k_1 \sin\theta_1 = k\sin\theta = k\nu$	
azimuthal angle	φ	

mismatch at the boundaries of the sample. The latter effect has been the subject of much activity recently [22–26].

The goal of the present paper is to extend our investigations to the multiple scattering of electromagnetic waves, obtaining thus for the first time a complete analytic description of the diffuse intensity and of the backscattering cone in the regime $\lambda \ll \ell \ll L$, including both polarization effects and internal reflections. We shall restrict the analysis to Rayleigh scatterers for definiteness. Section 2 contains general results on vector RTT. The observables of interest, with their dependence on polarizations and index mismatch, are expressed in terms of solutions of appropriate Schwarzschild-Milne equations. Sum rules and other general properties are given. These predictions are then made more quantitative in two situations: a) in the absence of internal reflections (Sect. 3), where a full analytical solution of the problem is given; the results of references [1,17,18] are made more precise and put in a broader perspective; b) in the opposite regime of a large mismatch of optical index between the sample and the surroundings (Sect. 4). Section 5 contains a brief discussion of our findings.

2. Generalities

2.1. General Formalism. — Throughout the following we consider the multiple scattering of electromagnetic waves by a diffusive medium containing a low density ρ of identical Rayleigh scatterers characterized by their cross-section σ, so that the mean free path $\ell = 1/(\rho\sigma)$ is much larger than the wavelength λ of radiation in the medium. The diffusive medium has the form of a slab ($0 < z < L$), infinite in the transverse directions. We introduce the optical thickness b of the sample through $L = b\ell$, and the optical depth τ of a point in the sample ($0 < \tau < b$) through $z = \tau\ell$. We shall consider either optically thick slabs ($b \gg 1$), or semi-infinite samples ($b = +\infty$). We investigate the general situation where the mean optical index n of the sample is different from that n_1 of the surrounding medium. Whenever there is an index mismatch ($m = n/n_1 \neq 1$), internal reflections take place at the boundaries of the sample. Useful definitions and notations are summarized in Table I.

We closely follow the definitions and notations of Chandrasekhar [1]. We measure the polarization of the radiation in a fixed frame, introducing spherical co-ordinates (see Tab. I). For radiation propagating in the angular direction (θ, φ) with respect to the z-axis, the complex components of the electric field $\mathbf{E}$ in the plane transversal to that direction will be denoted by (E_θ, E_φ). The component E_θ is parallel to the unit vector $\widehat{\boldsymbol{\theta}}$ and contained in the meridian plane, defined by the direction of propagation and the normal to the boundaries of the sample, while the component E_φ is parallel to the unit vector $\widehat{\boldsymbol{\varphi}}$ and normal to the meridian plane. The alternative notations $(E_\parallel, E_\perp)$ and (E_ℓ, E_r) can be found in the literature. We introduce the following vector of four Stokes parameters, or Stokes vector for short

$$\mathbf{I} : \begin{vmatrix} \mathbf{I}_1 = |E_\theta|^2 \\ \mathbf{I}_2 = |E_\varphi|^2 \\ \mathbf{I}_3 = U = 2\,\mathrm{Re}\,(E_\theta E_\varphi^*) \\ \mathbf{I}_4 = V = 2\,\mathrm{Im}\,(E_\theta E_\varphi^*). \end{vmatrix} \tag{2.1}$$

Here and throughout the following, boldface symbols represent 4-component vectors or 4×4 matrices. The description of polarized radiation by means of Stokes parameters is very commonly used [27]. This formalism has many advantages: the Stokes parameters add up for light beams superposed incoherently; a scattering event is described by a linear transformation of the Stokes parameters, *i.e.*, by the action of a scattering matrix on the Stokes vector $\mathbf{I}$. We finally recall the definition [27] of the degree of polarization P of radiation described by a Stokes vector $\mathbf{I}$:

$$P = \frac{\sqrt{(\mathbf{I}_1 - \mathbf{I}_2)^2 + U^2 + V^2}}{\mathbf{I}_1 + \mathbf{I}_2} \tag{2.2}$$

2.2. Schwarzschild-Milne Equation. — For reasons exposed in the Introduction, we shall use RTT to investigate the average reflected or transmitted intensity in the regime $\ell \gg \lambda$. We consider first the situation of a semi-infinite medium, for simplicity.

The mean diffuse radiation propagating in the direction (θ, φ) in the medium at depth $\tau = z/\ell$ is described by its Stokes vector $\mathbf{I}(\tau, \mu, \varphi)$, with the notations (see Tab. I)

$$\mu = \cos\theta, \quad \nu = \sin\theta = \sqrt{1 - \mu^2}. \tag{2.3}$$

Along the lines of reference [1], the RTT equation reads

$$\mu \frac{\partial}{\partial \tau} \mathbf{I}(\tau, \mu, \varphi) = \boldsymbol{\Gamma}(\tau, \mu, \varphi) - \mathbf{I}(\tau, \mu, \varphi), \tag{2.4}$$

where the vector source function $\boldsymbol{\Gamma}(\tau, \mu, \varphi)$ is defined as

$$\boldsymbol{\Gamma}(\tau, \mu, \varphi) = \int_{-1}^{1} \frac{\mathrm{d}\mu'}{2\mu'} \int_0^{2\pi} \frac{\mathrm{d}\varphi'}{2\pi} \mathbf{P}(\mu, \varphi, \mu', \varphi') \cdot \mathbf{I}(\tau, \mu', \varphi'), \tag{2.5}$$

with the Rayleigh phase matrix $\mathbf{P}(\mu, \varphi, \mu', \varphi')$ being the matrix describing a scattering event, expressed in the fixed frame related to the sample. Its explicit form will be given in equations (2.10, 2.11).

The RTT equation (2.4), with appropriate boundary conditions, leads to the following linear integral equation for the source function, referred to as the Schwarzschild-Milne (SM) equation

$$\begin{aligned}\mathbf{\Gamma}(\tau,\mu,\varphi) &= \mathbf{P}(\mu,\varphi,\mu_a,\varphi_a)\cdot\mathbf{I}_a e^{-\tau/\mu_a}\\ &+\int_0^{\tau}\mathrm{d}\tau'\int_0^1\frac{\mathrm{d}\mu'}{2\mu'}\int_0^{2\pi}\frac{\mathrm{d}\varphi'}{2\pi}e^{-(\tau-\tau')/\mu'}\mathbf{P}(\mu,\varphi,\mu',\varphi')\cdot\mathbf{\Gamma}(\tau',\mu',\varphi')\\ &+\int_{\tau}^{+\infty}\mathrm{d}\tau'\int_0^1\frac{\mathrm{d}\mu'}{2\mu'}\int_0^{2\pi}\frac{\mathrm{d}\varphi'}{2\pi}e^{-(\tau'-\tau)/\mu'}\mathbf{P}(\mu,\varphi,-\mu',\varphi')\cdot\mathbf{\Gamma}(\tau',-\mu',\varphi')\\ &+\int_0^{+\infty}\mathrm{d}\tau'\int_0^1\frac{\mathrm{d}\mu'}{2\mu'}\int_0^{2\pi}\frac{\mathrm{d}\varphi'}{2\pi}e^{-(\tau+\tau')/\mu'}\mathbf{R}(\mu')\cdot\mathbf{P}(\mu,\varphi,\mu',\varphi')\cdot\mathbf{\Gamma}(\tau',\mu',\varphi'). \quad (2.6)\end{aligned}$$

The right-hand side of this equation has the following interpretation:

- the first line is the exponentially damped contribution, with a suitable normalization [19,20], of the incident beam, characterized by an incident direction (θ_a,φ_a) and a Stokes vector $\mathbf{I}_a$;
- the second (third) line is the *bulk* contribution of diffuse light scattered from a smaller (larger) depth τ';
- the fourth line is the *layer* contribution of diffuse light scattered from depth τ' and then reflected at the boundary ($\tau = 0$). The effect of the boundary is described by a reflection matrix $\mathbf{R}(\mu)$ and a transmission matrix $\mathbf{T}(\mu)$, namely

$$\mathbf{R}(\mu) = \begin{pmatrix} |r_{\parallel}(\mu)|^2 & 0 & 0 & 0\\ 0 & |r_{\perp}(\mu)|^2 & 0 & 0\\ 0 & 0 & \mathrm{Re}\big(r_{\parallel}(\mu)r_{\perp}(\mu)^*\big) & -\mathrm{Im}\big(r_{\parallel}(\mu)r_{\perp}(\mu)^*\big)\\ 0 & 0 & \mathrm{Im}\big(r_{\parallel}(\mu)r_{\perp}(\mu)^*\big) & \mathrm{Re}\big(r_{\parallel}(\mu)r_{\perp}(\mu)^*\big)\end{pmatrix}, \quad (2.7)$$

$$\mathbf{T}(\mu) = \frac{m\mu}{\sqrt{1-m^2\nu^2}}\begin{pmatrix} |t_{\parallel}(\mu)|^2 & 0 & 0 & 0\\ 0 & |t_{\perp}(\mu)|^2 & 0 & 0\\ 0 & 0 & \mathrm{Re}\big(t_{\parallel}(\mu)t_{\perp}(\mu)^*\big) & -\mathrm{Im}\big(t_{\parallel}(\mu)t_{\perp}(\mu)^*\big)\\ 0 & 0 & \mathrm{Im}\big(t_{\parallel}(\mu)t_{\perp}(\mu)^*\big) & \mathrm{Re}\big(t_{\parallel}(\mu)t_{\perp}(\mu)^*\big)\end{pmatrix}.$$

In these expressions $r_{\parallel}(\mu)$, $r_{\perp}(\mu)$ and $t_{\parallel}(\mu)$, $t_{\perp}(\mu)$ are the Fresnel reflection and transmission amplitude coefficients, respectively. The latter only depend on the inner incidence angle θ and on the index mismatch m, according to

$$\begin{aligned} r_{\parallel}(\mu) &= \frac{\mu - m\sqrt{1-m^2\nu^2}}{\mu + m\sqrt{1-m^2\nu^2}}, \quad r_{\perp}(\mu) = \frac{\sqrt{1-m^2\nu^2} - m\mu}{\sqrt{1-m^2\nu^2} + m\mu},\\ t_{\parallel}(\mu) &= \frac{2\sqrt{1-m^2\nu^2}}{\mu + m\sqrt{1-m^2\nu^2}}, \quad t_{\perp}(\mu) = \frac{2\sqrt{1-m^2\nu^2}}{\sqrt{1-m^2\nu^2} + m\mu} \end{aligned} \quad (2.8)$$

In the case of partial reflection (see Tab. I), these coefficients are real, with absolute values less than unity. In the case of total reflection, the reflection coefficients are pure phases, *i.e.*, complex numbers with unit modulus, while the transmission coefficients vanish by convention. The first two diagonal elements of the reflection matrix $\mathbf{R}(\mu)$ of equation (2.7) read

$$|r_{\parallel}(\mu)|^2 = R_{\parallel}(\mu) = 1 - T_{\parallel}(\mu), \quad |r_{\perp}(\mu)|^2 = R_{\perp}(\mu) = 1 - T_{\perp}(\mu), \quad (2.9)$$

in terms of the Fresnel reflection and transmission intensity coefficients.

It is advantageous to expand the φ-dependence of all quantities in the complex trigonometric polynomials $\{e^{ik\varphi}\}$, with $-2 \leq k \leq 2$. We thus set

$$\mathbf{I}(\mu,\varphi) = \sum_{k=-2}^{2} \mathbf{I}^{(k)}(\mu) e^{ik\varphi}, \quad \mathbf{\Gamma}(\mu,\varphi) = \sum_{k=-2}^{2} \mathbf{\Gamma}^{(k)}(\mu) e^{ik\varphi},$$

$$\mathbf{P}(\mu,\varphi,\mu',\varphi') = \sum_{k=-2}^{2} \mathbf{P}^{(k)}(\mu,\mu') e^{ik(\varphi-\varphi')} \tag{2.10}$$

The Rayleigh phase matrices read

$$\mathbf{P}^{(0)}(\mu,\mu') = \frac{3}{4}\begin{pmatrix} 2(1-\mu^2)(1-\mu'^2)+\mu^2\mu'^2 & \mu^2 & 0 & 0 \\ \mu'^2 & 1 & 0 & 0 \\ 0 & 0 & 0 & 0 \\ 0 & 0 & 0 & 2\mu\mu' \end{pmatrix},$$

$$\mathbf{P}^{(1)}(\mu,\mu') = \mathbf{P}^{(-1)^*}(\mu,\mu') = \frac{3}{4}\nu\nu'\begin{pmatrix} 2\mu\mu' & 0 & i\mu & 0 \\ 0 & 0 & 0 & 0 \\ -2i\mu' & 0 & 1 & 0 \\ 0 & 0 & 0 & 1 \end{pmatrix},$$

$$\mathbf{P}^{(2)}(\mu,\mu') = \mathbf{P}^{(-2)^*}(\mu,\mu') = \frac{3}{8}\begin{pmatrix} \mu^2\mu'^2 & -\mu^2 & i\mu^2\mu' & 0 \\ -\mu'^2 & 1 & -i\mu' & 0 \\ -2i\mu\mu'^2 & 2i\mu & 2\mu\mu' & 0 \\ 0 & 0 & 0 & 0 \end{pmatrix}, \tag{2.11}$$

and the SM equation (2.6) splits into the following five decoupled integral equations $(-2 \leq k \leq 2)$

$$\begin{aligned} \mathbf{\Gamma}^{(k)}(\tau,\mu) \;=\; & \mathbf{P}^{(k)}(\mu,\mu_a)\cdot\mathbf{I}_a e^{-ik\varphi_a-\tau/\mu_a} \\ & + \int_0^{\tau} d\tau' \int_0^1 \frac{d\mu'}{2\mu'} e^{-(\tau-\tau')/\mu'} \mathbf{P}^{(k)}(\mu,\mu')\cdot\mathbf{\Gamma}^{(k)}(\tau',\mu') \\ & + \int_{\tau}^{+\infty} d\tau' \int_0^1 \frac{d\mu'}{2\mu'} e^{-(\tau'-\tau)/\mu'} \mathbf{P}^{(k)}(\mu,-\mu')\cdot\mathbf{\Gamma}^{(k)}(\tau',-\mu') \\ & + \int_0^{+\infty} d\tau' \int_0^1 \frac{d\mu'}{2\mu'} e^{-(\tau+\tau')/\mu'} \mathbf{R}(\mu')\cdot\mathbf{P}^{(k)}(\mu,\mu')\cdot\mathbf{\Gamma}^{(k)}(\tau',\mu'). \end{aligned} \tag{2.12}$$

2.3. Solutions to the SM Equation and Sum Rules. — We now turn to the analysis of the solutions to the SM equation (2.6). We shall investigate their general symmetry properties, and show that they obey some remarkable sum rules.

We start by introducing the matrix Green's function $\mathbf{G}(\tau,\mu,\varphi,\tau',\mu',\varphi')$, defined as being the solution, which remains bounded as either τ or τ' goes to infinity, of the SM equation with a matrix δ-function source term, namely

$$\begin{aligned} & \mathbf{G}(\tau,\mu,\varphi,\tau',\mu',\varphi') = \mathbf{P}(\mu,\varphi,\mu',\varphi')\delta(\tau-\tau') \\ & + \int_0^{\tau} d\tau'' \int_0^1 \frac{d\mu''}{2\mu''} \int_0^{2\pi} \frac{d\varphi''}{2\pi} e^{-(\tau-\tau'')/\mu''} \mathbf{P}(\mu,\varphi,\mu'',\varphi'')\cdot\mathbf{G}(\tau'',\mu'',\varphi'',\tau',\mu',\varphi') \\ & + \int_{\tau}^{+\infty} d\tau'' \int_0^1 \frac{d\mu''}{2\mu''} \int_0^{2\pi} \frac{d\varphi''}{2\pi} e^{-(\tau''-\tau)/\mu''} \mathbf{P}(\mu,\varphi,-\mu'',\varphi'')\cdot\mathbf{G}(\tau'',-\mu'',\varphi'',\tau',\mu',\varphi') \\ & + \int_0^{+\infty} d\tau'' \int_0^1 \frac{d\mu''}{2\mu''} \int_0^{2\pi} \frac{d\varphi''}{2\pi} e^{-(\tau+\tau'')/\mu''} \mathbf{R}(\mu'')\cdot\mathbf{P}(\mu,\varphi,\mu'',\varphi'')\cdot\mathbf{G}(\tau'',\mu'',\varphi'',\tau',\mu',\varphi'). \end{aligned} \tag{2.13}$$

The source function $\mathbf{\Gamma}(\tau,\mu,\varphi)$, solution of the SM equation (2.6), is then given by

$$\mathbf{\Gamma}(\tau,\mu,\varphi) = \mathbf{\Gamma}(\tau,\mu,\varphi,\mu_a,\varphi_a)\cdot\mathbf{I}_a, \tag{2.14}$$

where

$$\mathbf{\Gamma}(\tau,\mu,\varphi,\mu_a,\varphi_a) = \int_0^{+\infty} \mathrm{d}\tau' \mathrm{e}^{-\tau'/\mu_a}\mathbf{G}(\tau,\mu,\varphi,\tau',\mu_a,\varphi_a). \tag{2.15}$$

We also define the matrix of bistatic coefficients, or bistatic matrix for short

$$\begin{aligned}\gamma(\mu_a,\varphi_a,\mu_b,\varphi_b) &= \int_0^{+\infty} \mathrm{d}\tau\, \mathrm{e}^{-\tau/\mu_b}\mathbf{\Gamma}(\tau,-\mu_b,\varphi_b,\mu_a,\varphi_a)\\ &= \int_0^{+\infty} \mathrm{d}\tau\, \mathrm{e}^{-\tau/\mu_b}\int_0^{+\infty} \mathrm{d}\tau'\, \mathrm{e}^{-\tau'/\mu_a}\mathbf{G}(\tau,-\mu_b,\varphi_b,\tau',\mu_a,\varphi_a).\end{aligned} \tag{2.16}$$

The invariance of the Rayleigh scattering mechanism under time reversal implies the following symmetry properties of the quantities defined so far. We introduce the constant matrices

$$\mathbf{K} = \begin{pmatrix} 1 & 0 & 0 & 0\\ 0 & 1 & 0 & 0\\ 0 & 0 & 1/2 & 0\\ 0 & 0 & 0 & 1/2\end{pmatrix}, \quad \mathbf{L} = \begin{pmatrix} 1 & 0 & 0 & 0\\ 0 & 1 & 0 & 0\\ 0 & 0 & -1/2 & 0\\ 0 & 0 & 0 & 1/2\end{pmatrix}, \tag{2.17}$$

the matrix $\mathbf{K}$ being denoted by $\mathbf{Q}^{-1}$ in reference [1]. The Rayleigh phase matrix $\mathbf{P}(\mu,\varphi,\mu',\varphi')$ has the symmetry property $(i,j=1,\cdot\quad,4)$

$$\begin{aligned}(\mathbf{K}\cdot\mathbf{P})_{ij}(\mu,\varphi,\mu',\varphi') &= (\mathbf{K}\cdot\mathbf{P})_{ji}(\mu',\varphi',\mu,\varphi),\\ (\mathbf{L}\cdot\mathbf{P})_{ij}(\mu,\varphi,\mu',\varphi') &= (\mathbf{L}\cdot\mathbf{P})_{ji}(-\mu',\varphi',-\mu,\varphi).\end{aligned} \tag{2.18}$$

It then follows from their definitions (2.13, 2.16) that the matrix Green's function and the bistatic matrix obey the symmetry relations $(i,j=1,\cdot\quad,4)$

$$\begin{aligned}(\mathbf{K}\cdot\mathbf{G})_{ij}(\tau,\mu,\varphi,\tau'.\mu',\varphi') &= (\mathbf{K}\cdot\mathbf{G})_{ji}(\tau',\mu',\varphi',\tau,\mu,\varphi),\\ (\mathbf{L}\cdot\mathbf{G})_{ij}(\tau,\mu,\varphi,\tau'.\mu',\varphi') &= (\mathbf{L}\cdot\mathbf{G})_{ji}(\tau',-\mu',\varphi',\tau.-\mu,\varphi),\\ (\mathbf{L}\cdot\gamma)_{ij}(\mu,\varphi,\mu',\varphi') &= (\mathbf{L}\cdot\gamma)_{ji}(\mu',\varphi',\mu,\varphi).\end{aligned} \tag{2.19}$$

We now investigate the asymptotic behaviour of quantities deep inside the medium, *i.e.*, for $\tau\to+\infty$. It is expected on physical grounds that the diffusive medium depolarises the incident radiation, so that both $\mathbf{I}(\tau,\mu,\varphi)$ and $\mathbf{\Gamma}(\tau,\mu,\varphi)$ become proportional to the Stokes vector of natural (unpolarized) light, namely [27]

$$\mathbf{I}_{\mathrm{nat}} = \begin{pmatrix}1\\1\\0\\0\end{pmatrix}. \tag{2.20}$$

This assertion will be made quantitative in Section 3, where the extinction lengths of the all other modes will be determined. The asymptotic behaviour of the matrix solution $\mathbf{\Gamma}(\tau,\mu,\varphi,\mu_a,\varphi_a)$ then assumes the form

$$\mathbf{\Gamma}(\tau,\mu,\varphi,\mu_a,\varphi_a)\to\begin{pmatrix}\tau_1(\mu_a) & \tau_2(\mu_a) & 0 & 0\\ \tau_1(\mu_a) & \tau_2(\mu_a) & 0 & 0\\ 0 & 0 & 0 & 0\\ 0 & 0 & 0 & 0\end{pmatrix} \quad (\tau\to+\infty). \tag{2.21}$$

Furthermore it should be noticed that the homogeneous SM equation (2.6, 2.12), without a source term, has a vector solution $\mathbf{\Gamma}_H(\tau,\mu)$ in the φ-independent ($k=0$) sector, growing linearly as $\tau \to +\infty$. We shall refer to the latter solution, normalized as

$$\mathbf{\Gamma}_H(\tau,\mu) \approx (\tau+\tau_0)\mathbf{I}_{\rm nat}, \tag{2.22}$$

as the homogeneous solution, for short.

The constant τ_0 and the functions $\tau_1(\mu)$ and $\tau_2(\mu)$, which show up in equations (2.22, 2.21), respectively, are unknown so far. It will be shown that they bear the full non-trivial dependence of the physical observables on the index mismatch. They will also be determined analytically in the absence of internal reflections (Sect. 3) and in the large index mismatch regime (Sect. 4).

For the time being, we pursue our investigation of general properties. The special and homogeneous solutions to the SM equation in the $k=0$ sector can be related among themselves as follows. The column vectors of the matrix Green's function obeying equation (2.13) become proportional to the homogeneous solution, as either τ or τ' goes to infinity:

$$\lim_{\tau'\to+\infty} \mathbf{G}^{(0)}_{ij}(\tau,\mu,\tau',\mu') = \frac{1}{2D}(\mathbf{\Gamma}_H)_i(\tau,\mu) \quad (i,j=1,\cdot\quad,4), \tag{2.23}$$

where the constant D will be determined and interpreted in a while. As a consequence of the above definitions, we have

$$\tau_i(\mu_a) = \lim_{\mu_b\to+\infty} \frac{\gamma^{(0)}_{ij}(\mu_a,\mu_b)}{\mu_b} = \frac{1}{2D}\int_0^{+\infty} \mathrm{d}\tau\, \mathrm{e}^{-\tau/\mu_a}(\mathbf{\Gamma}_H)_i(\tau,-\mu_a) \quad (i,j=1,2). \tag{2.24}$$

We end up by deriving two groups of sum rules obeyed by the quantities defined above, which are related to the F- and K-integrals, with the notations of reference [1].

• First, we consider the F-integral, defined as

$$F(\tau) = \int_{-1}^{1} \frac{\mathrm{d}\mu}{2}\mu \int_0^{2\pi} \frac{\mathrm{d}\varphi}{2\pi}\Big(\mathbf{I}_1(\tau,\mu,\varphi) + \mathbf{I}_2(\tau,\mu,\varphi)\Big). \tag{2.25}$$

The RTT equation (2.4) implies $\mathrm{d}F/\mathrm{d}\tau = 0$, expressing thus the conservation of the flux in the z-direction. We consider first the F-integrals F_1 and F_2 associated with the special solutions $\mathbf{\Gamma}_{i1}$ and $\mathbf{\Gamma}_{i2}$, *i.e.*, the first two column vectors of the matrix (2.15). The $\tau \to +\infty$ limit determines $F_1 = F_2 = 0$; the $\tau = 0$ values then yield the sum rules

$$\begin{aligned}
\int_0^1 \frac{\mathrm{d}\mu}{2}\Big[T_\parallel(\mu)\gamma^{(0)}_{11}(\mu,\mu_a) + T_\perp(\mu)\gamma^{(0)}_{12}(\mu,\mu_a)\Big] &= \mu_a,\\
\int_0^1 \frac{\mathrm{d}\mu}{2}\Big[T_\parallel(\mu)\gamma^{(0)}_{21}(\mu,\mu_a) + T_\perp(\mu)\gamma^{(0)}_{22}(\mu,\mu_a)\Big] &= \mu_a.
\end{aligned} \tag{2.26}$$

The $\mu_a \to +\infty$ limit of these equations, using equation (2.24), yields

$$\int_0^1 \frac{\mathrm{d}\mu}{2}\Big[T_\parallel(\mu)\tau_1(\mu) + T_\perp(\mu)\tau_2(\mu)\Big] = 1. \tag{2.27}$$

Similarly, we consider the F-integral F_H associated with the homogeneous solution $\mathbf{\Gamma}_H$. This does not yield any independent sum rule, but rather leads to the determination of the unknown constant D, namely

$$D = \frac{1}{3}, \tag{2.28}$$

to be interpreted as the dimensionless diffusion constant, *i.e.*, $D_{\rm phys} = c\ell/3$ in physical units.
• Second, we consider the K-integral, defined as

$$K(\tau) = \int_{-1}^{1} \frac{\mathrm{d}\mu}{2}\mu^2 \int_0^{2\pi} \frac{\mathrm{d}\varphi}{2\pi}\Big(\mathbf{I}_1(\tau,\mu,\varphi) + \mathbf{I}_2(\tau,\mu,\varphi)\Big). \tag{2.29}$$

The RTT equation (2.4) implies $\mathrm{d}K/\mathrm{d}\tau = -F$, whence $K(\tau) = -F\tau + K_0$, with K_0 being a constant. Along the lines of the above derivation, we obtain the sum rules

$$\begin{aligned}
\int_0^1 \frac{\mathrm{d}\mu}{2}\mu\Big[\big(1+R_\parallel(\mu)\big)\gamma_{11}^{(0)}(\mu,\mu_a) + \big(1+R_\perp(\mu)\big)\gamma_{12}^{(0)}(\mu,\mu_a)\Big] &= \frac{2}{3}\tau_1(\mu_a) + \mu_a^2,\\
\int_0^1 \frac{\mathrm{d}\mu}{2}\mu\Big[\big(1+R_\parallel(\mu)\big)\gamma_{21}^{(0)}(\mu,\mu_a) + \big(1+R_\perp(\mu)\big)\gamma_{22}^{(0)}(\mu,\mu_a)\Big] &= \frac{2}{3}\tau_2(\mu_a) + \mu_a^2,
\end{aligned} \tag{2.30}$$

and

$$\int_0^1 \frac{\mathrm{d}\mu}{2}\mu\Big[\big(1+R_\parallel(\mu)\big)\tau_1(\mu) + \big(1+R_\perp(\mu)\big)\tau_2(\mu)\Big] = \tau_0. \tag{2.31}$$

The sum rules (2.30, 2.31) express that the multiple-scattering problem in a semi-infinite sample is invariant if a finite slab of any thickness is added, or removed, from the sample [1].

2.4. Diffuse Reflected Intensity. — The diffuse reflected intensity for a semi-infinite sample can now be calculated, along the lines of references [19–21]. The incident radiation is characterized by the direction (θ_a, φ_a) and the Stokes vector $\mathbf{I}_a$; the reflected radiation is detected in the direction (θ_b, φ_b) and in a polarization state characterized by the Stokes vector $\mathbf{I}_b$. Our prediction for the mean reflected intensity per solid-angle element reads

$$\frac{\mathrm{d}R(a\to b)}{\mathrm{d}\Omega_b} = A^{\rm R}(\theta_a,\varphi_a,\theta_b,\varphi_b) = \frac{\cos\theta_a}{4\pi m^2 \mu_a \mu_b}\big\langle \mathbf{I}_b\big|\mathbf{T}(\mu_b)\cdot\mathbf{L}\cdot\gamma(\mu_a,\varphi_a,\mu_b,\varphi_b)\cdot\mathbf{T}(\mu_a)\big|\mathbf{I}_a\big\rangle. \tag{2.32}$$

In the absence of index mismatch we obtain the simpler expression

$$A^{\rm R}(\theta_a,\varphi_a,\theta_b,\varphi_b) = \frac{1}{4\pi\mu_b}\big\langle \mathbf{I}_b\big|\mathbf{L}\cdot\gamma(\mu_a,\varphi_a,\mu_b,\varphi_b)\big|\mathbf{I}_a\big\rangle. \tag{2.33}$$

2.5. Diffuse Transmitted Intensity. — The diffuse transmitted intensity through an optically thick slab ($b \gg 1$) can also be calculated along the lines of references [19–21]. A first step consists in building up the solution $\mathbf{\Gamma}(b,\tau,\mu,\varphi,\mu_a,\varphi_a)$ of the SM equation pertaining to the thick-slab geometry. This solution can be expressed in terms of the solutions $\mathbf{\Gamma}(\tau,\mu,\varphi,\mu_a,\varphi_a)$ and $\mathbf{\Gamma}_H(\tau,\mu)$ pertaining to the semi-infinite geometry, by means of a matching procedure. It turns out that only the (1, 2) sector of the matrix solution matters, since all the other matrix elements are exponentially small in the optical thickness b. We thus get $(i,j=1,2)$

$$\mathbf{\Gamma}_{ij}(b,\tau,\mu,\varphi,\mu_a,\varphi_a) \approx \begin{cases} \mathbf{\Gamma}_{ij}(\tau,\mu,\varphi,\mu_a,\varphi_a) - \dfrac{\tau_i(\mu_a)}{b+2\tau_0}(\mathbf{\Gamma}_H)_i(\tau,\mu) & (\tau \text{ finite},\ b-\tau \gg 1),\\[2ex] \dfrac{\tau_i(\mu_a)}{b+2\tau_0}(\mathbf{\Gamma}_H)_i(b-\tau,-\mu) & (b-\tau \text{ finite},\ \tau \gg 1). \end{cases} \tag{2.34}$$

Both expressions lead to a linear (diffusive) behaviour in the bulk of the sample ($\tau \gg 1$, $b-\tau \gg 1$), namely

$$\mathbf{\Gamma}_{ij}(b,\tau,\mu,\varphi,\mu_a,\varphi_a) \approx \frac{b+\tau_0-\tau}{b+2\tau_0}\tau_i(\mu_a) \quad (i,j=1,2). \tag{2.35}$$

The mean diffuse transmitted intensity through an optically thick slab can then be derived explicitly, again along the lines of references [19–21]. The incident radiation is characterized by the direction (θ_a, φ_a) and the Stokes vector $\mathbf{I}_a$. The transmitted radiation is detected in the direction (θ_b, φ_b) and in a polarization state characterized by the Stokes vector $\mathbf{I}_b$. Our prediction for the mean transmitted intensity per solid-angle element reads

$$\frac{\mathrm{d}T(a \to b)}{\mathrm{d}\Omega_b} = \frac{A^{\mathrm{T}}(\theta_a, \theta_b)}{b + 2\tau_0}, \tag{2.36}$$

with

$$A^{\mathrm{T}}(\theta_a, \theta_b) = \frac{\cos\theta_a}{12\pi m^2 \mu_a \mu_b} \langle \mathbf{I}_b | \mathbf{A}(\mu_a, \mu_b) | \mathbf{I}_a \rangle. \tag{2.37}$$

The matrix $\mathbf{A}(\mu_a, \mu_b)$ has non-zero elements only in the (1, 2)-sector, namely

$$\mathbf{A}(\mu_a, \mu_b) = \begin{pmatrix} T_{\parallel}(\mu_a)\tau_1(\mu_a)T_{\parallel}(\mu_b)\tau_1(\mu_b) & T_{\parallel}(\mu_a)\tau_1(\mu_a)T_{\perp}(\mu_b)\tau_2(\mu_b) & 0 & 0 \\ T_{\perp}(\mu_a)\tau_2(\mu_a)T_{\parallel}(\mu_b)\tau_1(\mu_b) & T_{\perp}(\mu_a)\tau_2(\mu_a)T_{\perp}(\mu_b)\tau_2(\mu_b) & 0 & 0 \\ 0 & 0 & 0 & 0 \\ 0 & 0 & 0 & 0 \end{pmatrix}. \tag{2.38}$$

2.6. Enhanced Backscattering Cone

2.6.1. Generalities. — In the regime $\lambda \ll \ell$ of interest, the enhanced backscattering phenomenon takes place in a narrow cone around the exact backscattering direction, of angular width of order λ/ℓ. As recalled in the Introduction, the shape of the cone of enhanced backscattering for a semi-infinite medium is given by the sum of the cyclical, or maximally-crossed, diagrams. This summation can be performed by means of an adaptation of RTT. This property has been exploited extensively in the case of scalar waves [6, 7, 19–21]; it has been extended more recently to polarization effects for electromagnetic waves [17, 18].

We restrict ourselves to a semi-infinite medium and to normal incidence ($\theta_a = 0$). We define the dimensionless transverse wavevector of the outgoing radiation as

$$\mathbf{Q} = \mathbf{q}\ell, \tag{2.39}$$

with a magnitude

$$Q = q\ell = k\ell\theta = k_1\ell\theta_1, \tag{2.40}$$

with θ_1 being the observation angle. We assume for definiteness that the vector $\mathbf{Q}$ is parallel to the x-axis, namely $\mathbf{Q} = Q\hat{\mathbf{x}}$, with $Q \geq 0$. In order to cure the ill-definedness of the co-ordinate system at strictly normal incidence, we choose to give the initial wavevector an infinitesimally small positive component along $\hat{\mathbf{x}}$. We thus set $\theta_a = 0^+$, $\varphi_a = 0$, so that $\widehat{\boldsymbol{\theta}} = \hat{\mathbf{x}}$ and $\widehat{\boldsymbol{\varphi}} = \hat{\mathbf{y}}$. We then introduce a Q-dependent matrix of bistatic coefficients, $\gamma_{ij}(Q, \mu_a, \varphi_a, \mu_b, \varphi_b)$. The latter is defined, in analogy with equation (2.16), in terms of the matrix source function $\boldsymbol{\Gamma}_{ij}(Q, \mu, \varphi, \mu_a, \varphi_a)$. This matrix solves the Q-dependent SM equation, obtained by replacing in equation (2.13) the exponential damping factor $\exp(-\tau/\mu')$ by $\exp\big(-(1 - i\mathbf{Q}\cdot\mathbf{n})\tau/\mu'\big)$, where $\mathbf{n}$ is the unit vector in the direction (θ', φ'), so that $\mathbf{Q}\cdot\mathbf{n} = Q\nu'\cos\varphi'$.

We now turn to the explicit shape of the enhanced backscattering cone. It can be expressed [17, 18] in terms of the values at normal incidence of the bistatic coefficients, $\gamma_{ij}(Q) = \gamma_{ij}(Q, \mu_a = 1, \varphi_a = 0, \mu_b = 1, \varphi_b = 0)$. To be more specific, the total reflected intensity near the backscattering direction, *i.e.*, for $\theta \ll 1$, $k\ell \gg 1$, and $Q = k\ell\theta \geq 0$ fixed, reads

$$A(Q) = A^{\mathrm{L}} + A^{\mathrm{C}}(Q) - A^{\mathrm{SS}} = \frac{4}{\pi(m+1)^4} \langle \mathbf{I}_b | \mathbf{L} \cdot \big(\gamma^{\mathrm{L}} + \gamma^{\mathrm{C}}(Q) - \gamma^{\mathrm{SS}}\big) | \mathbf{I}_a \rangle. \tag{2.41}$$

• The first term in equation (2.41), given by the sum of the ladder diagrams, coincides with the expression (2.32) for the background reflected intensity. At normal incidence it assumes the general form

$$\gamma^{\mathrm{L}} = \gamma(\mu_a = 1, \varphi_a = 0, \mu_b = 1, \varphi_b = 0) = \begin{pmatrix} \gamma_{11} & \gamma_{12} & 0 & 0 \\ \gamma_{12} & \gamma_{11} & 0 & 0 \\ 0 & 0 & \gamma_{12} - \gamma_{11} & 0 \\ 0 & 0 & 0 & \gamma_{44} \end{pmatrix}, \tag{2.42}$$

where the three constants γ_{11}, γ_{12}, and γ_{44} only depend on the index mismatch.

• The second term in equation (2.41) is given by the sum of the maximally crossed, or cyclical, diagrams. It represents the contributions of the interference between the sequences of any number ($N \geq 1$) of scattering events and their time-reversed counterparts. At normal incidence we have [17,18]

$$\gamma^{\mathrm{C}}(Q) = \begin{pmatrix} \gamma_{11}(Q) & \widetilde{\gamma}_{12}(Q) & 0 & 0 \\ \widetilde{\gamma}_{12}(Q) & \gamma_{22}(Q) & 0 & 0 \\ 0 & 0 & \widetilde{\gamma}_{33}(Q) & 0 \\ 0 & 0 & 0 & \widetilde{\gamma}_{44}(Q) \end{pmatrix}, \tag{2.43}$$

with

$$\begin{aligned} \widetilde{\gamma}_{12}(Q) &= \frac{1}{2}\big(\gamma_{44}(Q) - \gamma_{33}(Q)\big), \\ \widetilde{\gamma}_{33}(Q) &= \frac{1}{2}\big(\gamma_{33}(Q) + \gamma_{44}(Q)\big) - \gamma_{12}(Q), \\ \widetilde{\gamma}_{44}(Q) &= \frac{1}{2}\big(\gamma_{33}(Q) + \gamma_{44}(Q)\big) + \gamma_{12}(Q). \end{aligned} \tag{2.44}$$

• The subtracted third term in equation (2.41) is the contribution of the single-scattering ($N = 1$) events, which are their own time-reversed counterparts, and must not be double-counted. At normal incidence it reads

$$\gamma^{\mathrm{SS}} = \frac{3}{4}\begin{pmatrix} 1 & 0 & 0 & 0 \\ 0 & 1 & 0 & 0 \\ 0 & 0 & -1 & 0 \\ 0 & 0 & 0 & -1 \end{pmatrix}. \tag{2.45}$$

The actual calculation of the Q-dependent bistatic matrix $\gamma(Q, \mu_a, \varphi_a, \mu_b, \varphi_b)$ goes as follows. By expanding the Q-dependent SM equation in the trigonometric polynomials $\{\mathrm{e}^{\imath k\varphi}\}$, we obtain the following system of coupled equations ($-2 \leq k \leq 2$)

$$\begin{aligned} &\mathbf{\Gamma}^{(k)}(\tau, \mu) = \mathbf{P}^{(k)}(\mu, \mu_a) \cdot \mathbf{I}_a \mathrm{e}^{-\imath k\varphi_a - \tau/\mu_a} \\ &+ \int_0^{\tau} \mathrm{d}\tau' \int_0^1 \frac{\mathrm{d}\mu'}{2\mu'} \mathrm{e}^{-(\tau-\tau')/\mu'} \mathbf{P}^{(k)}(\mu, \mu') \cdot \sum_{j=-2}^{2} i^{k-j} J_{k-j}\big(Q(\tau - \tau')\nu'/\mu'\big) \mathbf{\Gamma}^{(j)}(\tau', \mu') \\ &+ \int_{\tau}^{\infty} \mathrm{d}\tau' \int_0^1 \frac{\mathrm{d}\mu'}{2\mu'} \mathrm{e}^{-(\tau'-\tau)/\mu'} \mathbf{P}^{(k)}(\mu, -\mu') \cdot \sum_{j=-2}^{2} i^{k-j} J_{k-j}\big(Q(\tau' - \tau)\nu'/\mu'\big) \mathbf{\Gamma}^{(j)}(\tau', -\mu') \\ &+ \int_0^{\infty} \mathrm{d}\tau' \int_0^1 \frac{\mathrm{d}\mu'}{2\mu'} \mathrm{e}^{-(\tau+\tau')/\mu'} \mathbf{R}(\mu') \cdot \mathbf{P}^{(k)}(\mu, \mu') \cdot \sum_{j=-2}^{2} i^{k-j} J_{k-j}\big(Q(\tau + \tau')\nu'/\mu'\big) \mathbf{\Gamma}^{(j)}(\tau', \mu'), \end{aligned} \tag{2.46}$$

where ν has been defined in equation (2.3), and where the $J_n(z)$ are the Bessel functions, which admit the integral representation

$$i^n J_n(z) = \int_0^{2\pi} \frac{\mathrm{d}\varphi}{2\pi} \exp\bigl(iz\cos\varphi - in\varphi\bigr), \tag{2.47}$$

and possess the symmetry property

$$J_{-n}(z) = J_n(-z) = (-1)^n J_n(z). \tag{2.48}$$

2.6.2. Linear Polarizations. — We now investigate the case where the initial beam is linearly polarized, and a linear polarization of the outgoing beam is detected. Let ψ_a and ψ_b be the respective angles between the directions of the polarizations and the direction of the **Q**-vector, *i.e.*, the positive x-axis. The corresponding Stokes vectors read

$$\mathbf{I}_a = \begin{pmatrix} \cos^2\psi_a \\ \sin^2\psi_a \\ \sin(2\psi_a) \\ 0 \end{pmatrix}, \quad \mathbf{I}_b = \begin{pmatrix} \cos^2\psi_b \\ \sin^2\psi_b \\ \sin(2\psi_b) \\ 0 \end{pmatrix}. \tag{2.49}$$

By inserting these expressions into the results (2.41–45), we obtain that A^{L} and A^{SS} only depend on the relative angle

$$\Psi = \psi_b - \psi_a \tag{2.50}$$

between the directions of both polarizations, namely

$$\begin{aligned} A^{\mathrm{L}} &= \frac{4}{\pi(m+1)^4}\bigl(\gamma_{11}\cos^2\Psi + \gamma_{12}\sin^2\Psi\bigr), \\ A^{\mathrm{SS}} &= \frac{3}{\pi(m+1)^4}\cos^2\Psi, \end{aligned} \tag{2.51}$$

whereas $A^{\mathrm{C}}(Q)$ depends separately on both polarization directions:

$$\begin{aligned} A^{\mathrm{C}}(Q) = \frac{4}{\pi(m+1)^4}\Bigl[&\gamma_{11}(Q)\cos^2\psi_a\cos^2\psi_b + \gamma_{22}(Q)\sin^2\psi_a\sin^2\psi_b \\ &+\bigl(2\gamma_{12}(Q) - \gamma_{33}(Q) - \gamma_{44}(Q)\bigr)\cos\psi_a\sin\psi_a\cos\psi_b\sin\psi_b \\ &+\frac{1}{2}\bigl(\gamma_{44}(Q) - \gamma_{33}(Q)\bigr)\bigl(\sin^2\psi_a\cos^2\psi_b + \sin^2\psi_b\cos^2\psi_a\bigr)\Bigr]. \end{aligned} \tag{2.52}$$

We define as usual the enhancement factor $B(Q)$ as the ratio between the total reflected intensity and its background value:

$$B(Q) = \frac{A^{\mathrm{L}} + A^{\mathrm{C}}(Q) - A^{\mathrm{SS}}}{A^{\mathrm{L}}} \tag{2.53}$$

Right at the top of the backscattering cone, corresponding to the exact backscattering direction ($Q = 0$), the expressions (2.41, 2.43) simplify to

$$A^{\mathrm{C}}(0) = \frac{4}{\pi(m+1)^4}\Bigl(\gamma_{11} - \frac{1}{2}(\gamma_{11} + \gamma_{12} - \gamma_{44})\sin^2\Psi\Bigr). \tag{2.54}$$

The enhancement factor thus reads

$$B(0) = \frac{\left(2\gamma_{11} - \frac{3}{4}\right) + \frac{1}{2}\left(-3\gamma_{11} + \gamma_{12} + \gamma_{44} + \frac{3}{2}\right)\sin^2\Psi}{\gamma_{11} + (\gamma_{12} - \gamma_{11})\sin^2\Psi}. \tag{2.55}$$

The maximal enhancement factor $B_{\parallel}$ is observed for parallel detection, *i.e.*, $\Psi = 0$, whereas the minimum $B_{\perp}$ corresponds to perpendicular detection, *i.e.*, $\Psi = \pm\pi/2$. These extremal values read

$$B_{\parallel} = 2 - \frac{3}{4\gamma_{11}}, \quad B_{\perp} = \frac{\gamma_{11} + \gamma_{12} + \gamma_{44}}{2\gamma_{12}} \tag{2.56}$$

A celebrated and universal feature of the enhanced backscattering cone is the triangular shape of its top. Within the present formalism, and in analogy with previous studies [19–21], this phenomenon is described as follows. For $Q \ll 1$, and for $i, j = 1, 2$, the solution $\mathbf{\Gamma}^{(0)}_{ij}(Q, \tau, \mu)$ of the Q-dependent SM equation has a term linear in Q that is proportional to the homogeneous solution $(\mathbf{\Gamma}_H)_i(\tau, \mu)$, namely

$$\mathbf{\Gamma}_{ij}(Q, \tau, \mu) = \mathbf{\Gamma}_{ij}(\tau, \mu) - C_i\, Q(\mathbf{\Gamma}_H)_i(\tau, \mu) + \mathcal{O}(Q^2) \quad (i, j = 1, 2). \tag{2.57}$$

The constants C_i are then fixed by requiring that the above solution falls off as $\exp(-Q\tau)$ for $Q\tau \gg 1$. This general property will be checked explicitly in Section 3 in the absence of internal reflections. We thus obtain $C_1 = C_2 = \tau_1(1) = \tau_2(1)$, so that

$$\gamma_{ij}(Q) = \gamma_{ij} - \frac{2}{3}\tau_1(1)^2\, Q + \mathcal{O}(Q^2) \quad (i, j = 1, 2), \tag{2.58}$$

and finally

$$A^{\mathrm{C}}(Q) = \frac{4}{\pi(m+1)^4}\left(\gamma_{11} - \frac{1}{2}(\gamma_{11} + \gamma_{22} - \gamma_{44})\sin^2\Psi - \frac{2}{3}\tau_1(1)^2\cos^2\Psi\, Q + \mathcal{O}(Q^2)\right). \tag{2.59}$$

Along the lines of references [19–21], we define the width ΔQ of the triangular cone as

$$A^{\mathrm{C}}(Q) = A^{\mathrm{C}}(0)\left(1 - \frac{Q}{\Delta Q} + \mathcal{O}(Q^2)\right). \tag{2.60}$$

The sharpest cone, namely the smallest width ΔQ, is observed for parallel detection, *i.e.*, $\Psi = 0$, where we have

$$\Delta Q_{\parallel} = \frac{3\gamma_{11}}{2\tau_1(1)^2}. \tag{2.61}$$

The universal features of the top of the enhanced backscattering cone described so far only depend on Q and Ψ. The full shape of the enhancement factor $B(Q)$ weakly depends separately on the directions ψ_a and ψ_b of both polarizations. This phenomenon will be illustrated in Section 3.2 in the absence of internal reflections.

2.6.3. Circular Polarizations. — We end up by investigating the case of circularly polarized beams at normal incidence. The corresponding Stokes vectors now read

$$\mathbf{I}_a = \begin{pmatrix} 1/2 \\ 1/2 \\ 0 \\ \sigma_a \end{pmatrix}, \quad \mathbf{I}_b = \begin{pmatrix} 1/2 \\ 1/2 \\ 0 \\ \sigma_b \end{pmatrix}, \tag{2.62}$$

where the helicity is $\sigma_a = 1$ (respectively, $\sigma_a = -1$) if the incident beam has a left (respectively, right) circular polarization, and similarly for the helicity σ_b of the detection channel. By inserting these expressions into the results (2.41–45), we observe that the various backscattered amplitudes only depend on the relative helicity

$$\Sigma = \sigma_a \sigma_b, \tag{2.63}$$

according to

$$\begin{aligned} A^{\mathrm{SS}} &= \frac{3}{\pi(m+1)^4}(1-\Sigma), \\ A^{\mathrm{L}} &= \frac{2}{\pi(m+1)^4}(\gamma_{11}+\gamma_{12}+\gamma_{44}\Sigma), \\ A^{\mathrm{C}}(Q) &= \frac{1}{\pi(m+1)^4}\Big[\gamma_{11}(Q)+\gamma_{22}(Q)-\gamma_{33}(Q)+\gamma_{44}(Q) \\ &\quad +\big(2\gamma_{12}(Q)+\gamma_{33}(Q)+\gamma_{44}(Q)\big)\Sigma\Big]. \end{aligned} \tag{2.64}$$

The enhancement factor $B_\Sigma(Q)$, defined in analogy with equation (2.53), is larger for the helicity-preserving channel ($\Sigma = 1$) than in the channel of opposite helicity ($\Sigma = -1$). In particular, right at the top of the cone, we have

$$B_1 = 2, \quad B_{-1} = \frac{3\gamma_{11} - \gamma_{12} - \gamma_{44} - 3/2}{\gamma_{11} + \gamma_{12} - \gamma_{44}} \tag{2.65}$$

The maximal value of the enhancement factor in the helicity-preserving channel is exactly equal to two, because $A^{\mathrm{L}} = A^{\mathrm{C}}(0)$ and the single-scattering contribution vanishes. Corrections to this exact factor of two for denser diffusive media (ℓ/λ not very large) have been measured in a recent experiment [28], and given a theoretical interpretation in terms of recurrent double scattering [29].

Another consequence of the result (2.64) is that the characteristic triangular shape of the cone only shows up in the helicity-preserving channel. The associated width, defined in analogy with equation (2.60), reads

$$\Delta Q_1 = \frac{3(\gamma_{11}+\gamma_{12}+\gamma_{44})}{4\tau_1(1)^2} \tag{2.66}$$

3. Exact Solution in the Absence of Internal Reflections

This section is devoted to the exact solution of the various SM equations introduced in Section 2, in the case where there is no optical index mismatch between the sample and the surroundings, so that there are no internal reflections: the reflection matrix $\mathbf{R}(\mu)$ vanishes. Therefore the SM equations (2.6, 2.12, 2.46) involve convolution kernels, which only depend on the difference of optical depths $\tau - \tau'$. The problem is, however, still non-trivial because of the semi-infinite geometry ($0 < \tau < +\infty$). We have found it worthwhile to expose a self-contained derivation of the Wiener-Hopf technique, and of the results known previously, and already exposed in the book by Chandrasekhar [1].

The vector RTT problem is considered in Section 3.1. The outcomes concerning diffuse reflection and transmission are compared in detail with those corresponding to multiple isotropic scattering of scalar waves [19, 20]. Section 3.2 deals with the enhanced backscattering phenomenon. We derive closed-form expressions for the five functions describing the full shape of the enhanced backscattering cone, up to the numerical solution of the 9×9 system (3.74). The present analysis thus goes one step further than the recent work by Ozrin [18].

3.1. DIFFUSE REFLECTION AND TRANSMISSION. — In this section we derive the exact solution to the SM equations (2.6, 2.12) in the absence of internal reflections, obtaining thus predictions for the diffuse reflected and transmitted intensity. We introduce the following parametrization

$$\mathbf{\Gamma}^{(0)}(\tau,\mu) = \begin{pmatrix} A(\tau) + B(\tau)(1-\mu^2) \\ A(\tau) \\ 0 \\ C(\tau)\mu \end{pmatrix},$$

$$\mathbf{\Gamma}^{(1)}(\tau,\mu) = \mathbf{\Gamma}^{(-1)^*}(\tau,\mu) = \nu \begin{pmatrix} D(\tau)\mu \\ 0 \\ -iD(\tau) \\ E(\tau) \end{pmatrix},$$

$$\mathbf{\Gamma}^{(2)}(\tau,\mu) = \mathbf{\Gamma}^{(-2)^*}(\tau,\mu) = F(\tau) \begin{pmatrix} \mu^2 \\ -1 \\ -2i\mu \\ 0 \end{pmatrix}, \tag{3.1}$$

where ν has been defined in equation (2.3). The functions $A(\tau), \cdot \quad , F(\tau)$ obey the integral equations

$$\begin{cases} A = \frac{3}{4}\Big((\mu_a^2\mathbf{I}_1 + \mathbf{I}_2)\mathrm{e}^{-\tau/\mu_a} + (M_0 + M_2) \star A + (M_2 - M_4) \star B\Big), \\ B = \frac{3}{4}\Big(((2-3\mu_a^2)\mathbf{I}_1 - \mathbf{I}_2)\mathrm{e}^{-\tau/\mu_a} + (M_0 - 3M_2) \star A + (2M_0 - 5M_2 + 3M_4) \star B\Big), \end{cases}$$

$$C = \frac{3}{2}\Big(\mu_a\mathbf{I}_4\mathrm{e}^{-\tau/\mu_a} + M_2 \star C\Big),$$

$$D = \frac{3}{4}\Big(\nu_a(2\mu_a\mathbf{I}_1 + i\mathbf{I}_3)\mathrm{e}^{-\tau/\mu_a} + (M_0 + M_2 - 2M_4) \star D\Big),$$

$$E = \frac{3}{4}\Big(\nu_a\mathbf{I}_4\mathrm{e}^{-\tau/\mu_a} + (M_0 - M_2) \star E\Big),$$

$$F = \frac{3}{8}\Big((\mu_a^2\mathbf{I}_1 - \mathbf{I}_2 + i\mu_a\mathbf{I}_3)\mathrm{e}^{-\tau/\mu_a} + (M_0 + 2M_2 + M_4) \star F\Big), \tag{3.2}$$

where the brace shows that the equations for $A(\tau)$ and $B(\tau)$ are coupled, while the other four are decoupled. In the above equations, the star denotes the convolution between a kernel $M(\tau - \tau')$ and a function $A(\tau)$, defined as

$$(M \star A)(\tau) = \int_0^{+\infty} M(\tau - \tau')A(\tau')\mathrm{d}\tau'. \tag{3.3}$$

The kernels entering equation (3.2) are the following even functions

$$M_{2p}(\tau) = \int_0^1 \frac{\mathrm{d}\mu}{2\mu}\mu^{2p}\mathrm{e}^{-|\tau|/\mu} \tag{3.4}$$

3.1.1. Preliminaries. — As recalled above, the integral equations (3.2) are exactly solvable because of their convolution structure, which suggests to utilize the Laplace transformation. Along the lines of references [19–21], the Laplace transform of a function $A(\tau)$ defined for $0 < \tau < +\infty$ will be denoted by $a(s)$ (the corresponding lower-case letter), and defined as

$$a(s) = \int_0^{+\infty} A(\tau)\mathrm{e}^{s\tau}\mathrm{d}\tau, \tag{3.5}$$

while the Laplace transform of the kernels $M_{2p}(\tau)$ read

$$m_{2p}(s) = \int_{-\infty}^{+\infty} M_{2p}(\tau) e^{s\tau} d\tau = \int_0^1 d\mu \frac{\mu^{2p}}{1 - s^2\mu^2}, \tag{3.6}$$

i.e., explicitly,

$$\begin{aligned} m_0(s) &= \frac{1}{2s} \ln \frac{1+s}{1-s}, \\ m_2(s) &= \frac{1}{s^2}(m_0(s) - 1), \\ m_4(s) &= \frac{1}{s^4}\left(m_0(s) - 1 - \frac{s^2}{3}\right). \end{aligned} \tag{3.7}$$

We also define for further use the following linear combinations of the above kernels

$$\begin{aligned} \phi_1(s) &= 1 - \frac{3}{4}(m_0(s) - m_2(s)), \\ \phi_2(s) &= -\frac{1}{s^2}\left[1 - \frac{3}{2}(m_0(s) - m_2(s))\right], \\ \phi_3(s) &= 1 - \frac{3}{4}(m_0(s) + m_2(s) - 2m_4(s)), \\ \phi_4(s) &= 1 - \frac{3}{8}(m_0(s) + 2m_2(s) + m_4(s)), \\ \phi_5(s) &= 1 - \frac{3}{2}m_2(s), \end{aligned} \tag{3.8}$$

which we shall refer to as the kernel functions. Both the kernels $m_{2p}(s)$ and the kernel functions $\phi_n(s)$ are even functions of s, analytic in the s-plane cut along the real axis from $-\infty$ to -1 and from $+1$ to $+\infty$.

In the following we shall need to factorize the $\phi_n(s)$ into the corresponding so-called Wiener-Hopf H-functions, defined from reference [1] by the identity

$$\phi_n(s) = \frac{1}{H_n(s)H_n(-s)} \quad (n = 1, \cdot \quad , 5), \tag{3.9}$$

together with the condition that $H_n(s)$ is analytic in the left half-plane $\mathrm{Re}\, s < 0$. Consider first the case of a rational function of the form

$$\phi(s) = \frac{\prod_{a=1}^{M}(s^2 - z_a^2)}{\prod_{b=1}^{N}(s^2 - p_b^2)}, \tag{3.10}$$

with $2M$ zeros and $2N$ poles at arbitrary positions, with $\mathrm{Re}\, z_a > 0$, $\mathrm{Re}\, p_b > 0$. The factorization (3.9) is elementary in this case, and the associated H-function reads

$$H(s) = \frac{\prod_{b=1}^{N}(s - p_b)}{\prod_{a=1}^{M}(s - z_a)} \tag{3.11}$$

This expression can be recast as a complex contour integral, yielding thus an explicit representation of the H-functions in the general case:

$$H_n(s) = \exp\left(\int \frac{\mathrm{d}z}{2\pi i}\,\frac{\phi_n'(z)}{\phi_n(z)}\,\ln(z-s)\right) = \exp\left(-\int \frac{\mathrm{d}z}{2\pi i}\,\frac{\ln\phi_n(z)}{z-s}\right) \quad (\mathrm{Re}\, s < 0), \tag{3.12}$$

where the vertical contour can be placed at $\mathrm{Re}\, z = 0$. In the present case it is advantageous, especially for the purpose of numerical evaluation, to change variables from z to an angle β such that $z = i\tan\beta$. We thus get

$$H_n(s) = \exp\left(\frac{s}{\pi}\int_0^{\pi/2} \mathrm{d}\beta \frac{\ln\widetilde{\phi}_n(\beta)}{\sin^2\beta + s^2\cos^2\beta}\right) \quad (\mathrm{Re}\, s < 0), \tag{3.13}$$

with

$$\begin{aligned}
\widetilde{\phi}_1(\beta) &= 1 - \frac{3}{4}\Big((\cot^2\beta+1)(\beta\cot\beta - 1) + 1\Big),\\
\widetilde{\phi}_2(\beta) &= \cot^2\beta\left[1 - \frac{3}{2}\Big((\cot^2\beta+1)(\beta\cot\beta-1)+1\Big)\right],\\
\widetilde{\phi}_3(\beta) &= 1 + \frac{3}{4}\Big((2\cot^4\beta + \cot^2\beta - 1)(\beta\cot\beta - 1) + \frac{2}{3}\cot^2\beta - 1\Big),\\
\widetilde{\phi}_4(\beta) &= 1 - \frac{3}{8}\Big((\cot^2\beta - 1)^2(\beta\cot\beta - 1) + \frac{1}{3}\cot^2\beta + 1\Big),\\
\widetilde{\phi}_5(\beta) &= 1 + \frac{3}{2}\cot^2\beta(\beta\cot\beta - 1).
\end{aligned} \tag{3.14}$$

The following values of the H-functions will play a role hereafter. First, the kernel functions have the following series expansions around the origin

$$\begin{aligned}
&\phi_1(s) = \frac{1}{2} - \frac{1}{10}s^2 + \cdot \quad , \quad \phi_2(s) = \frac{1}{5} + \frac{3}{35}s^2 + \cdot \quad , \quad \phi_3(s) = \frac{3}{10} - \frac{13}{70}s^2 + \cdot \quad ,\\
&\phi_4(s) = \frac{3}{10} - \frac{23}{70}s^2 + \cdot \quad , \quad \phi_5(s) = \frac{1}{2} - \frac{3}{10}s^2 + \cdot
\end{aligned} \tag{3.15}$$

Equation (3.9) yields $H_n(0) = 1/\sqrt{\phi_n(0)}$, hence

$$H_1(0) = \sqrt{2}, \quad H_2(0) = \sqrt{5}, \quad H_3(0) = H_4(0) = \sqrt{\frac{10}{3}}, \quad H_5(0) = \sqrt{2}. \tag{3.16}$$

Second, for large s, namely $|s| \to +\infty$ with $\mathrm{Re}\, s < 0$, the functions $H_n(s)$ with $n \neq 2$ go to unity, while we have $H_2(s) \approx -s$. Finally, the values of the H-functions at $s = -1$ can be accurately determined from the integral representation (3.13, 3.14). We thus obtain

$$\begin{aligned}
&H_1(-1) = 1.277\,973, \quad H_2(-1) = 3.469\,485, \quad H_3(-1) = 1.465\,877,\\
&H_4(-1) = 1.396\,266, \quad H_5(-1) = 1.203\,622.
\end{aligned} \tag{3.17}$$

3.1.2. Homogeneous SM Equation and Diffuse Transmission. — The solution to the homogeneous SM equation is *a priori* of the form

$$\mathbf{\Gamma}_H(\tau,\mu) = \begin{pmatrix} A_H(\tau) + B_H(\tau)(1-\mu^2) \\ A_H(\tau) \\ 0 \\ 0 \end{pmatrix}. \tag{3.18}$$

We deduce from the integral equations (3.2) for the functions $A_H(\tau)$ and $B_H(\tau)$, in the absence of source terms, the following equations for their Laplace transforms $a_H(s)$ and $b_H(s)$

$$\left(\frac{4}{3} - m_0(s) - m_2(s)\right) a_H(s) + \big(m_4(s) - m_2(s)\big) b_H(s) = \mathcal{A}_H(s),$$

$$\big(3m_2(s) - m_0(s)\big) a_H(s) + \left(\frac{4}{3} - 2m_0(s) + 5m_2(s) + 3m_4(s)\right) b_H(s) = \mathcal{B}_H(s), \quad (3.19)$$

with right-hand sides

$$\mathcal{A}_H(s) = \int \frac{\mathrm{d}t}{2\pi i(t-s)} \Big[\big(m_0(t) + m_2(t)\big) a_H(t) + \big(m_2(t) - m_4(t)\big) b_H(t)\Big],$$

$$\mathcal{B}_H(s) = \int \frac{\mathrm{d}t}{2\pi i(t-s)} \Big[\big(m_0(t) - 3m_2(t)\big) a_H(t) + \big(2m_0(t) - 5m_2(t) - 3m_4(t)\big) b_H(t)\Big]. \quad (3.20)$$

On the other hand, the asymptotic behaviour (2.22) implies

$$a_H(s) = \frac{1}{s^2} - \frac{\tau_0}{s} + \mathcal{O}(1) \quad (s \to 0), \quad (3.21)$$

while $b_H(0)$ is expected to be finite in this limit.

The determinant of the 2×2 linear system (3.19) can be factorized as $(16/9)\phi_1(s)\phi_2(s)$. This system can be put in diagonal form by looking for linear combinations of the lines of equation (3.19) involving only $\phi_1(s)$ or $\phi_2(s)$ acting on the unknowns. We thus get

$$\phi_1(s) a_H(s) = \frac{3}{8s^2}\Big((3 - 2s^2)\mathcal{A}_H(s) + \mathcal{B}_H(s)\Big), \quad (3.22a)$$

$$\phi_2(s)\Big((1 - s^2) b_H(s) - s^2 a_H(s)\Big) = \frac{3}{4}\Big(\mathcal{A}_H(s) + \mathcal{B}_H(s)\Big). \quad (3.22b)$$

We now solve these equations by means of the so-called Wiener-Hopf technique. We consider first equation (3.22a), and we start by investigating the case where $\phi_1(s)$ is a rational function of the form (3.10), with zeros at $s = \pm z_{1,a}$ and poles at $s = \pm p_{1,b}$. We observe that $a_H(s)$ is regular for $\mathrm{Re}\, s < 0$, while the right-hand side of equation (3.22a) is regular for $\mathrm{Re}\, s > 0$. Moreover, equation (3.20) implies that this right-hand side grows at most linearly as $s \to -\infty$. Hence the solution of equation (3.22a), normalized by the condition (3.21), reads

$$a_H(s) = \frac{1 - cs}{s^2} \frac{\displaystyle\prod_{b=1}^{N} (1 - s/p_{1,b})}{\displaystyle\prod_{a=1}^{N} (1 - s/z_{1,a})} = \frac{1 - cs}{s^2} \frac{H_1(s)}{\sqrt{2}}, \quad (3.23)$$

where c is a constant, yet to be determined. Similarly, the solution of equation (3.22b) reads

$$b_H(s) = \frac{1}{1 - s^2}\left((1 - cs)\frac{H_1(s)}{\sqrt{2}} - qH_2(s)\right), \quad (3.24)$$

where q is another constant. The notation c and q follows reference [1]. These two constants are determined by expressing that the right-hand side of equation (3.24) remains finite as $s \to \pm 1$. We finally obtain

$$c = \frac{2H_2^2(-1) - H_1^2(-1)}{H_1^2(-1) + 2H_2^2(-1)}, \quad q = \frac{2\sqrt{2}H_1(-1)H_2(-1)}{H_1^2(-1) + 2H_2^2(-1)}. \quad (3.25)$$

Table II. — *Comparison of various quantities of interest, defined in Section 2, from the known exact solutions in the absence of internal reflections. First row: isotropic scattering of scalar waves, from reference [19]. Second row: Rayleigh scattering of electromagnetic waves (Sect. 3 of this work). Third row: relative difference of second case with respect to first one.*

	isotropic scattering (scalar waves)	Rayleigh scattering (electromagnetic waves)	$\Delta(\%)$
skin layer thickness	$\tau_0 = 0.710\,446$	$\tau_0 = 0.712\,110$	0.23
diffuse transmission	$\frac{1}{2}\tau_{\rm scal}(1) = 2.518\,237$	$\tau_i(1) = 2.538\,761 \quad (i = 1, 2)$	0.81
diffuse reflection	$\gamma(1,1) = 4.227\,681$	$\gamma_{11} + \gamma_{12} = 4.588\,369$	8.5
enhancement at top of cone	$B = 1.881\,732$	$B_\parallel = 1.752\,088$	−6.9
		$B_1 = 2$	6.3
width of top of cone	$\Delta Q = 1/2$	$\Delta Q_\parallel = 0.704\,063$	41
		$\Delta Q_1 = 0.407\,487$	−19

The representation (3.13, 3.14) permits a numerical evaluation of these numbers, and of all the subsequent quantities, with arbitrary accuracy. We thus get

$$c = 0.872\,941, \quad q = 0.487\,827. \tag{3.26}$$

It is worth noticing that the exact solution derived above does not require to determine the auxiliary functions $\mathcal{A}_H(s)$ and $\mathcal{B}_H(s)$ explicitly.

The observables of interest can now be deduced as follows.

• The constant τ_0 is obtained by comparing the result (3.23) with the expansion (3.21), namely

$$\tau_0 = c - \frac{H_1'(0)}{\sqrt{2}} = 0.712\,110. \tag{3.27}$$

This number is remarkably close to the celebrated value for isotropic scattering of scalar waves, recalled in Table II.

• The functions $\tau_1(\mu)$ and $\tau_2(\mu)$ are obtained from their definition (2.24), yielding

$$\tau_1(\mu) = \frac{3}{2}\Big(a_H(-1/\mu) + (1-\mu^2)b_H(-1/\mu)\Big), \quad \tau_2(\mu) = \frac{3}{2}a_H(-1/\mu), \tag{3.28}$$

i.e., explicitly,

$$\tau_1(\mu) = \frac{3}{2}q\mu^2 H_2(-1/\mu), \quad \tau_2(\mu) = \frac{3}{2\sqrt{2}}\mu(\mu + c)H_1(-1/\mu). \tag{3.29}$$

In order to make a comparison with the case of scalar waves, we must take into account that the above results describe a single polarization state, and should be compared with *half* the corresponding quantity for isotropic scattering of scalar waves, determined in references [19,20], and denoted there by $\tau_1(\mu)$, and hereafter by $\tau_{\rm scal}(\mu)$. At nearly grazing incidence, both

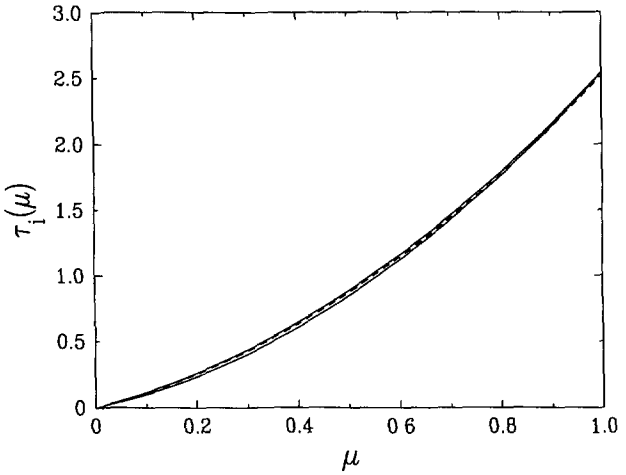

Fig. 1. — Plot of angular dependence of transmitted intensity in the absence of internal reflections, against $\mu = \cos\theta$. Full lines: $\tau_1(\mu)$ (lower curve) and $\tau_2(\mu)$ (upper curve), corresponding to both polarizations channels for Rayleigh scattering (this work). Dashed line: $\tau_{\rm scal}(\mu)/2$, corresponding to half the result for isotropic scattering of scalar waves, from reference [19].

functions $\tau_1(\mu)$ and $\tau_2(\mu)$ vanish linearly, according to

$$\tau_1(\mu) \approx \frac{3}{2} q\mu = 0.731\,740\,\mu, \quad \tau_2(\mu) \approx \frac{3}{2\sqrt{2}} c\mu = 0.925\,893\,\mu, \tag{3.30}$$

while in the scalar case we have $\tau_{\rm scal}(\mu)/2 \approx (\sqrt{3}/2)\mu = 0.866\,025\,\mu$. At normal incidence, both functions take the common value

$$\tau_1(1) = \tau_2(1) = \frac{3\sqrt{2} H_1(-1) H_2^2(-1)}{H_1^2(-1) + 2H_2^2(-1)} = 2.538\,761, \tag{3.31}$$

which is again very close to the corresponding number in the case of scalar waves (see Tab. II). The full functions $\tau_1(\mu)$ and $\tau_2(\mu)$ are plotted in Figure 1. They hardly differ from each other, and from half the corresponding scalar quantity $\tau_{\rm scal}(\mu)/2$.

In order to underline the main novelty with respect to the scalar case [19, 20], namely polarization effects, we plot in Figure 2 the degree of polarization P, defined in equation (2.2), which reads in the present case

$$P(\mu) = \frac{\tau_2(\mu) - \tau_1(\mu)}{\tau_2(\mu) + \tau_1(\mu)}. \tag{3.32}$$

This quantity has a maximum at grazing incidence, namely

$$P(0) = \frac{c - q\sqrt{2}}{c + q\sqrt{2}} = 0.117\,127, \tag{3.33}$$

and vanishes at normal incidence, as it should.

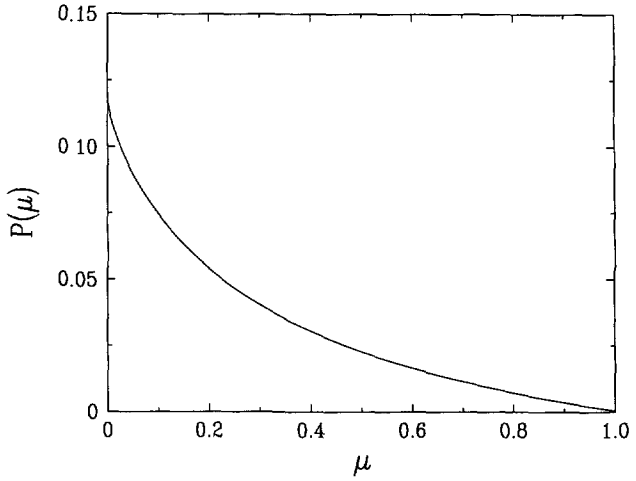

Fig. 2. — Plot of angular dependence of degree of polarization $P(\mu)$ of diffuse transmitted intensity, in the absence of internal reflections, against $\mu = \cos\theta$.

3.1.3. Inhomogeneous SM Equation and Diffuse Reflection. — The special solution of the full inhomogeneous SM equation can be derived by solving the six equations (3.2), along the lines of the previous subsection.

Let us begin with the functions $A(\tau)$ and $B(\tau)$. Their Laplace transforms $a(s)$ and $b(s)$ still obey equations of the form (3.19), albeit with the contributions of the source terms in their right-hand sides:

$$\begin{aligned}
\mathcal{A}(s) &= (\mu_a^2\mathbf{I}_1 + \mathbf{I}_2)\frac{\mu_a}{1-s\mu_a} \\
&\quad + \int \frac{\mathrm{d}t}{2\pi i(t-s)}\Big[\big(m_0(t)+m_2(t)\big)a(t) + \big(m_2(t)-m_4(t)\big)b(t)\Big], \\
\mathcal{B}(s) &= \big((2-3\mu_a^2)\mathbf{I}_1 - \mathbf{I}_2\big)\frac{\mu_a}{1-s\mu_a} \\
&\quad + \int \frac{\mathrm{d}t}{2\pi i(t-s)}\Big[\big(m_0(t)-3m_2(t)\big)a(t) + \big(2m_0(t)-5m_2(t)-3m_4(t)\big)b(t)\Big]. \quad (3.34)
\end{aligned}$$

These equations can be solved by means of the Wiener-Hopf technique, along the lines of the previous subsection. The undetermined constants can be fixed in terms of c and q, given by equation (3.25), and we finally obtain

$$\begin{aligned}
a(s) &= -\frac{3\mu_a H_1(s)}{2\sqrt{2}s}\left(q\mu_a H_2(-1/\mu_a)\mathbf{I}_1 + \frac{\mu_a + c - (1+\mu_a c)s}{1-s\mu_a}\frac{H_1(-1/\mu_a)}{\sqrt{2}}\mathbf{I}_2\right), \\
b(s) &= \frac{1}{1-s^2}\Bigg[s^2 a(s) \\
&\quad - \frac{3\mu_a H_2(s)}{2}\left(\mu_a\frac{\mu_a - c - (1-\mu_a c)s}{1-s\mu_a}H_2(-1/\mu_a)\mathbf{I}_1 + q\frac{H_1(-1/\mu_a)}{\sqrt{2}}\mathbf{I}_2\right)\Bigg]. \quad (3.35)
\end{aligned}$$

The other four functions $C(\tau), \cdots, F(\tau)$ are easier to determine, since the last four lines of equation (3.2) are uncoupled. We thus obtain the following closed-form expressions for

their Laplace transforms

$$\begin{aligned} c(s) &= \frac{3}{2}\frac{\mu_a^2 \mathbf{I}_4}{1-s\mu_a} H_5(s)H_5(-1/\mu_a), \\ d(s) &= \frac{3}{4}\frac{\mu_a\nu_a(2\mu_a\mathbf{I}_1 + i\mathbf{I}_3)}{1-s\mu_a} H_3(s)H_3(-1/\mu_a), \\ e(s) &= \frac{3}{4}\frac{\mu_a\nu_a\mathbf{I}_4}{1-s\mu_a} H_1(s)H_1(-1/\mu_a), \\ f(s) &= \frac{3}{8}\frac{\mu_a(\mu_a^2\mathbf{I}_1 - \mathbf{I}_2 + i\mu_a\mathbf{I}_3)}{1-s\mu_a} H_4(s)H_4(-1/\mu_a). \end{aligned} \tag{3.36}$$

The above results (3.35, 3.36) allow us to give the following expression for the full bistatic matrix in the absence of internal reflections:

$$\gamma(\mu_a, \varphi_a, \mu_b, \varphi_b) = \sum_{k=-2}^{2} \gamma^{(k)}(\mu_a, \mu_b) e^{ik(\varphi_a - \varphi_b)}, \tag{3.37}$$

with

$$\gamma^{(0)}(\mu_a, \mu_b) = \frac{3}{2}\mu_a\mu_b \times \begin{pmatrix} \mu_a\mu_b\left(\dfrac{1+\mu_a\mu_b}{\mu_a+\mu_b} - c\right) H_2^a H_2^b & \dfrac{q\mu_b}{\sqrt{2}} H_1^a H_2^b & 0 & 0 \\ \dfrac{q\mu_a}{\sqrt{2}} H_2^a H_1^b & \frac{1}{2}\left(\dfrac{1+\mu_a\mu_b}{\mu_a+\mu_b} + c\right) H_1^a H_1^b & 0 & 0 \\ 0 & 0 & 0 & 0 \\ 0 & 0 & 0 & -\dfrac{\mu_a\mu_b}{\mu_a+\mu_b} H_5^a H_5^b \end{pmatrix},$$

$$\gamma^{(1)}(\mu_a, \mu_b) = \gamma^{(-1)^*}(\mu_a, \mu_b) = \frac{3}{4}\frac{\mu_a\nu_a\mu_b\nu_b}{\mu_a+\mu_b} \begin{pmatrix} -2\mu_a\mu_b H_3^a H_3^b & 0 & -i\mu_b H_3^a H_3^b & 0 \\ 0 & 0 & 0 & 0 \\ -2i\mu_a H_3^a H_3^b & 0 & H_3^a H_3^b & 0 \\ 0 & 0 & 0 & H_1^a H_1^b \end{pmatrix},$$

$$\gamma^{(2)}(\mu_a, \mu_b) = \gamma^{(-2)^*}(\mu_a, \mu_b) = \frac{3}{8}\frac{\mu_a\mu_b}{\mu_a+\mu_b} \begin{pmatrix} \mu_a^2\mu_b^2 & -\mu_b^2 & i\mu_a\mu_b^2 & 0 \\ -\mu_a^2 & 1 & -i\mu_a & 0 \\ 2i\mu_a^2\mu_b & -2i\mu_b & -2\mu_a\mu_b & 0 \\ 0 & 0 & 0 & 0 \end{pmatrix} H_4^a H_4^b, \tag{3.38}$$

and with the notation $H_n^a = H_n(-1/\mu_a)$, $H_n^b = H_n(-1/\mu_b)$.

At normal incidence ($\mu_a = \mu_b = 1$, $\varphi_a = \varphi_b = 0$), the above expression simplifies, and it agrees with the general form (2.42), with

$$\begin{aligned} \gamma_{11} &= \frac{3H_1^2(-1)H_2^2(-1)}{H_1^2(-1) + 2H_2^2(-1)} + \frac{3H_4^2(-1)}{8} = 3.025\,270, \\ \gamma_{12} &= \frac{3H_1^2(-1)H_2^2(-1)}{H_1^2(-1) + 2H_2^2(-1)} - \frac{3H_4^2(-1)}{8} = 1.563\,100, \\ \gamma_{44} &= -\frac{3H_5^2(-1)}{4} = -1.086\,530. \end{aligned} \tag{3.39}$$

We now derive a few special results of interest from the above general expressions. First, neglecting polarization effects, the total diffuse reflected intensity in the normal direction is given by

$$\gamma_{11} + \gamma_{12} = \frac{6H_1^2(-1)H_2^2(-1)}{H_1^2(-1) + 2H_2^2(-1)} = 4.588\,369. \tag{3.40}$$

This number is slightly above the corresponding value $\gamma(1,1)$ for isotropic scattering of scalar waves (see Tab. II).

The interesting polarization dependence of the enhancement factor at the top of the backscattering cone, described in general terms in Section 2.6, can also be made fully quantitative in the present case. For linearly polarized beams, the extremal enhancement factors (2.56), corresponding to parallel and perpendicular detection, read

$$B_{\|} = 1.752\,088, \quad B_{\perp} = 1.120\,158, \tag{3.41}$$

while the width of the triangular cone for parallel detection (2.61) is

$$\Delta Q_{\|} = 0.704\,063. \tag{3.42}$$

For circularly polarized beams, the enhancement factors (2.65) in the helicity-preserving channel and in the channel of opposite helicity read, respectively,

$$B_1 = 2, \quad B_{-1} = 1.250\,989, \tag{3.43}$$

while the width of the triangular cone in the helicity-preserving channel (2.66) is

$$\Delta Q_1 = 0.407\,487. \tag{3.44}$$

The most significant of these numbers are again compared with their analogues for isotropic scattering of scalar waves in Table II.

3.1.4. Extinction Lengths of Non-Diffusive Modes. — The exact solution of the inhomogeneous SM equation in the absence of internal reflections, derived in Section 3.1.3, also allows us to predict the extinction lengths characterizing the exponential fall-off of the various non-diffusive polarized components of the intensity of radiation, deep in the bulk of a semi-infinite sample. These quantities do not depend at all on the index mismatch, so that the results derived below are quite general.

Let us take for definiteness the example of the component of the intensity described by the function $D(\tau)$, defined in equation (3.1). Its Laplace transform $d(s)$ is by construction analytic for $\mathrm{Re}\, s < 0$. The explicit expression (3.36) shows, however, that it is actually analytic in a larger domain, defined by $\mathrm{Re}\, s < 1/\mu_a$ and $\mathrm{Re}\, s < s_3$, where s_3 is the first pole of $H_3(s)$, namely the first zero of the kernel function $\phi_3(s)$. Here *first* means *having the smallest real part*. We have $s_3 = 0.914\,815 < 1 \leq 1/\mu_a$. The first singularity of $d(s)$ is therefore a simple pole at $s = s_3$. We have thus demonstrated the exponential fall-off $D(\tau) \sim \exp(-\tau/\ell_3)$, with a dimensionless reduced extinction length $\ell_3 = 1/s_3 = 1.093\,116$.

More generally, all the extinction lengths are given by the locations of the first singularities of the corresponding Laplace transforms. We thus obtain

$$B(\tau) \sim E(\tau) \sim \mathrm{e}^{-\tau/\ell_1}, \quad C(\tau) \sim \mathrm{e}^{-\tau/\ell_5}, \quad D(\tau) \sim \mathrm{e}^{-\tau/\ell_3}, \quad F(\tau) \sim \mathrm{e}^{-\tau/\ell_4}, \tag{3.45}$$

while the function $A(\tau)$, pertaining to the diffusive sector, does not fall off, but it rather admits the limit value $A(+\infty) = \tau_1(\mu_a)\mathbf{I}_1 + \tau_2(\mu_a)\mathbf{I}_2$ deep inside a semi-infinite sample.

Thus there are altogether four different dimensionless extinction lengths, $\ell_n = 1/s_n$ ($n = 1, 3, 4, 5$), where s_n is the zero of the kernel function $\phi_n(s)$ having the smallest positive real part. Table III gives the exact values of the extinction lengths ℓ_n, together with the corresponding approximate values ℓ_n^{diff}, predicted by the diffusion approximation [10]. This approximate scheme consists in brutally truncating the kernel functions $\phi_n(s)$ to the second order of their series expansion in s, given in equation (3.15).

3.2. Enhanced Backscattering Peak. — We now derive analytical expressions for the five functions describing the polarization dependence of the enhanced backscattering cone at normal incidence, according to the general formalism exposed in Section 2.6, in the absence of internal reflections. We start by introducing the following parametrization

$$\mathbf{\Gamma}^{(0)}(\tau,\mu) = \begin{pmatrix} A(\tau) + B(\tau)(1-\mu^2) \\ A(\tau) \\ 0 \\ C(\tau)\mu \end{pmatrix},$$

$$\mathbf{\Gamma}^{(1)}(\tau,\mu) = -\mathbf{\Gamma}^{(-1)^*}(\tau,\mu) = \nu \begin{pmatrix} \big(iD(\tau) - E(\tau)\big)\mu \\ 0 \\ D(\tau) + iE(\tau) \\ iF(\tau) \end{pmatrix},$$

$$\mathbf{\Gamma}^{(2)}(\tau,\mu) = \mathbf{\Gamma}^{(-2)^*}(\tau,\mu) = \big(G(\tau) + iH(\tau)\big) \begin{pmatrix} \mu^2 \\ -1 \\ -2i\mu \\ 0 \end{pmatrix}, \tag{3.46}$$

that slightly differs from equation (3.1).

Table III. — *Dimensionless reduced extinction lengths of the various polarized components of the diffuse intensity. First row: exact extinction lengths, deduced in Section 3.1.4 from the solution to the SM equation. Second row: approximate extinction lengths, obtained by means of the diffusion approximation [10]. Third row: relative difference of second case with respect to first one. Fourth row: notations used in reference [10].*

exact	diffusion approximation	$\Delta(\%)$	notation of ref. [10]
$\ell_1 = 1$	$\ell_1^{\text{diff}} = \sqrt{\frac{1}{5}} = 0.447\,213$	-55	ℓ'_3
$\ell_3 = 1.093\,116$	$\ell_3^{\text{diff}} = \sqrt{\frac{13}{21}} = 0.786\,796$	-28	ℓ'_2
$\ell_4 = 1.349\,587$	$\ell_4^{\text{diff}} = \sqrt{\frac{23}{21}} = 1.046\,536$	-22	ℓ_2
$\ell_5 = 1.172\,669$	$\ell_5^{\text{diff}} = \sqrt{\frac{3}{5}} = 0.774\,596$	-34	ℓ_3

Equation (2.46) implies that the eight real functions $A(\tau), \cdot \quad , H(\tau)$ obey the following sets of coupled linear integral equations, as shown by the braces

$$\begin{cases} A = \frac{3}{4}\Big((\mathbf{I}_1 + \mathbf{I}_2)e^{-\tau} + (M_{00} + M_{02}) \star A + (M_{02} - M_{04}) \star B \\ \qquad - 2M_{13} \star D + 2(M_{20} + M_{22}) \star G\Big), \\ B = \frac{3}{4}\Big(-(\mathbf{I}_1 + \mathbf{I}_2)e^{-\tau} + (M_{00} - 3M_{02}) \star A + (2M_{00} - 5M_{02} + 3M_{04}) \star B \\ \qquad + 2(-2M_{11} + 3M_{13}) \star D - 2(M_{20} + 3M_{22}) \star G\Big), \\ D = \frac{3}{4}\Big(2M_{11} \star A + 2(M_{11} - M_{13}) \star B \\ \qquad + (M_{00} + M_{02} - 2M_{04} + M_{20} - 2M_{22}) \star D + 2(M_{11} + M_{13} + M_{31}) \star G\Big), \\ G = \frac{3}{8}\Big((\mathbf{I}_1 - \mathbf{I}_2)e^{-\tau} + M_{20} \star A - M_{22} \star B \\ \qquad - (M_{11} + M_{13} + M_{31}) \star D + (M_{00} + 2M_{02} + M_{04} + M_{40}) \star G\Big), \end{cases} \tag{3.47a}$$

$$\begin{cases} C = \frac{3}{2}\Big(\mathbf{I}_4 \mathrm{e}^{-\tau} + M_{02} \star C - 2M_{11} \star F\Big), \\ F = \frac{3}{4}\Big(M_{11} \star C + (M_{00} - M_{02} - M_{20}) \star F\Big), \end{cases} \tag{3.47b}$$

$$\begin{cases} E = \frac{3}{4}\Big((M_{00} + M_{02} - 2M_{04} - M_{20} + 2M_{22}) \star E + 2(M_{11} + M_{13} - M_{31}) \star H\Big), \\ H = \frac{3}{8}\Big(\mathbf{I}_3 \mathrm{e}^{-\tau} + (-M_{11} - M_{13} + M_{31}) \star E + (M_{00} + 2M_{02} + M_{04} - M_{40}) \star H\Big). \end{cases} \tag{3.47c}$$

The kernels involved in these equations read

$$M_{pq}(Q, \tau) = \int_0^1 \frac{\mathrm{d}\mu}{2\mu} \mu^p \nu^q \mathrm{e}^{-|\tau|/\mu} J_q\big(Q\nu|\tau|/\mu\big), \tag{3.48}$$

where ν has been defined in equation (2.3).

3.2.1. Preliminaries: Kernels and H-Functions. — The explicit solution of equation (3.47) again involves the Laplace transforms $a(s), \cdot \quad , h(s)$ of the functions introduced in the parametrization (3.46). In a first step, we must therefore evaluate the Laplace transforms $m_{pq}(Q, s)$ of the kernels $M_{pq}(Q, \tau)$. Let us take the example of $m_{00}(Q, s)$. The representation (3.48) yields

$$m_{00}(Q, s) = \underbrace{\int_{-1}^{1} \frac{\mathrm{d}\mu}{2} \int_0^{2\pi} \frac{\mathrm{d}\varphi}{2\pi}}_{\int \frac{\mathrm{d}\Omega}{4\pi}} \int_{-\infty}^{+\infty} \frac{\mathrm{d}\tau}{|\mu|} \Theta(\tau\mu) \exp\left(s\tau - \frac{\tau}{\mu} + iQ\frac{\nu\tau}{\mu} \sin\varphi\right), \tag{3.49}$$

where Θ is Heaviside's function, and $\mathrm{d}\Omega$ is the solid-angle element on the unit sphere of $\mathbf{n}$, with co-ordinates $X = \nu\cos\varphi = \sin\theta\cos\varphi$, $Y = \nu\sin\varphi = \sin\theta\sin\varphi$, $Z = \mu = \cos\theta$. Performing the τ-integral yields

$$m_{00}(Q, s) = \int \frac{\mathrm{d}\Omega}{4\pi} \frac{1}{1 - s\cos\theta - iQ\sin\theta\cos\varphi} \tag{3.50}$$

The denominator can be transformed by a suitable rotation in the Y-Z plane into $1 - \sigma Z'$, with

$$\sigma = \sqrt{s^2 - Q^2}. \tag{3.51}$$

We thus obtain

$$m_{00}(Q,s) = m_0(\sigma). \tag{3.52}$$

It turns out that all the kernels involved in equation (3.47) can be treated similarly, and expressed as linear combinations of the $m_{2p}(\sigma)$, which have been determined in equation (3.7), namely

$$\begin{aligned}
m_{00}(Q,s) &= m_0(\sigma), \\
m_{02}(Q,s) &= m_2(\sigma) + \frac{Q^2}{2\sigma^2}\big(3m_2(\sigma) - m_0(\sigma)\big), \\
m_{04}(Q,s) &= m_4(\sigma) + \frac{Q^2}{\sigma^2}\big(5m_4(\sigma) - 3m_2(\sigma)\big) + \frac{Q^4}{8\sigma^4}\big(35m_4(\sigma) - 30m_2(\sigma) + 3m_0(\sigma)\big), \\
m_{11}(Q,s) &= \frac{Qs}{2\sigma^2}\big(3m_2(\sigma) - m_0(\sigma)\big), \\
m_{13}(Q,s) &= \frac{Qs}{2\sigma^2}\big(5m_4(\sigma) - 3m_2(\sigma)\big) + \frac{Q^3 s}{8\sigma^4}\big(35m_4(\sigma) - 30m_2(\sigma) + 3m_0(\sigma)\big), \\
m_{20}(Q,s) &= \frac{Q^2}{2\sigma^2}\big(3m_2(\sigma) - m_0(\sigma)\big), \\
m_{22}(Q,s) &= \frac{Q^2}{4\sigma^2}\big(15m_4(\sigma) - 12m_2(\sigma) + m_0(\sigma)\big) + \frac{Q^4}{8\sigma^4}\big(35m_4(\sigma) - 30m_2(\sigma) + 3m_0(\sigma)\big), \\
m_{31}(Q,s) &= \frac{Q^3 s}{8\sigma^4}\big(35m_4(\sigma) - 30m_2(\sigma) + 3m_0(\sigma)\big), \\
m_{40}(Q,s) &= \frac{Q^4}{8\sigma^4}\big(35m_4(\sigma) - 30m_2(\sigma) + 3m_0(\sigma)\big).
\end{aligned} \tag{3.53}$$

We are again led to consider the kernel functions $\phi_n(\sigma)$, defined in equation (3.8). Although the latter only depend on the variable σ of equation (3.51), the associated H-functions $H_n(Q,s)$ depend separately on both variables Q and s. The latter functions are still defined by the Wiener-Hopf identity (3.9), which now reads

$$\phi_n(\sigma) = \frac{1}{H_n(Q,s)H_n(Q,-s)}, \tag{3.54}$$

with the condition that the $H_n(Q,s)$ be analytic in the left half-plane $\mathrm{Re}\, s < 0$. For a rational kernel function $\phi(\sigma)$ of the form (3.10), the H-function reads

$$H(Q,s) = \frac{\displaystyle\prod_{b=1}^{N}\left(s - \sqrt{Q^2 + p_b^2}\right)}{\displaystyle\prod_{a=1}^{M}\left(s - \sqrt{Q^2 + z_a^2}\right)} \tag{3.55}$$

In the present case, the functions $H_n(Q,s)$ still possess the integral representation (3.13), up to the replacement

$$\beta \to \widetilde{\beta}(Q,\beta) = \arctan\sqrt{Q^2 + \tan^2\beta}. \tag{3.56}$$

3.2.2. Derivation of $\gamma_{44}(Q)$. — We begin with the exact solution of the 2×2 system (3.47b), yielding, after a Laplace transformation, $c(Q,s)$ and $f(Q,s)$, and $\gamma_{44}(Q)$ through $c(Q,-1) = -\gamma_{44}(Q)\mathbf{I}_4$. The determinant of this linear system can be factorized as $-(9/8)\phi_1(\sigma)\phi_5(\sigma)$. Along the lines of Section 3.1, the system is made diagonal by setting

$$\begin{aligned} \widetilde{c}(Q,s) &= sc(Q,s) - 2Qf(Q,s), \\ \widetilde{f}(Q,s) &= (Q/2)c(Q,s) - sf(Q,s). \end{aligned} \tag{3.57}$$

The inverse formulae read

$$\begin{aligned} \sigma^2 c(Q,s) &= s\widetilde{c}(Q,s) - 2Q\widetilde{f}(Q,s), \\ \sigma^2 f(Q,s) &= (Q/2)\widetilde{c}(Q,s) - s\widetilde{f}(Q,s), \end{aligned} \tag{3.58}$$

and the new functions obey

$$\begin{aligned} \phi_5(\sigma)\widetilde{c}(Q,s) &= -\frac{s}{1-s}\mathbf{I}_4 + \widetilde{\mathcal{C}}(Q,s), \\ \phi_1(\sigma)\widetilde{f}(Q,s) &= \frac{Q}{1-s}\mathbf{I}_4 + \widetilde{\mathcal{F}}(Q,s), \end{aligned} \tag{3.59}$$

where $\widetilde{\mathcal{C}}(Q,s)$ and $\widetilde{\mathcal{F}}(Q,s)$ are defined in analogy with equation (3.20).

The solution of equation (3.59) reads

$$\begin{aligned} \widetilde{c}(Q,s) &= \left(c_1 + \frac{c_2}{1-s}\right)\mathbf{I}_4 H_5(Q,s), \\ \widetilde{f}(Q,s) &= \left(f_1 + \frac{f_2}{1-s}\right)\mathbf{I}_4 H_1(Q,s). \end{aligned} \tag{3.60}$$

This expression involves, besides the corresponding H-functions, four constants, yet to be determined. The $s \to 1$ limit of equation (3.59) fixes two of them:

$$c_2 = \frac{3}{2}\mathbf{I}_4 H_5(Q,-1), \quad f_2 = \frac{3}{4}Q\mathbf{I}_4 H_1(Q,-1). \tag{3.61}$$

The last two constants, c_1 and f_1, are then fixed by requiring that $c(Q,s)$ and $f(Q,s)$, as given by equation (3.58), are finite for $\sigma \to 0$, *i.e.*, $s \to Q$ and $s \to -Q$. Skipping lengthy details, we finally get

$$\gamma_{44}(Q) = -\frac{3}{4}\frac{\mathcal{N}_{44}(Q)}{(1-Q^2)^2\left(H_1^2(Q,-Q) + H_5^2(Q,-Q)\right)}, \tag{3.62}$$

where

$$\begin{aligned} \mathcal{N}_{44}(Q) = {} & Q^2(1+Q)^2 H_5^2(Q,-Q)H_1^2(Q,-1) + Q^2(1-Q)^2 H_1^2(Q,-Q)H_1^2(Q,-1) \\ & +(1-Q)^2 H_5^2(Q,-Q)H_5^2(Q,-1) + (1+Q)^2 H_1^2(Q,-Q)H_5^2(Q,-1) \\ & -8Q^2 H_1(Q,-Q)H_5(Q,-Q)H_1(Q,-1)H_5(Q,-1). \end{aligned} \tag{3.63}$$

3.2.3. Derivation of $\gamma_{33}(Q)$. — The 2×2 linear system (3.47c) yields, after a Laplace transformation, $e(Q,s)$ and $h(Q,s)$, and $\gamma_{33}(Q)$ through $h(Q,-1) = (1/4)\gamma_{33}(Q)\mathbf{I}_3$. The determinant of this system can be factorized as $(9/32)\phi_3(\sigma)\phi_4(\sigma)$. Its exact solution closely follows the lines of the previous subsection. We are led to consider the linear combinations

$$\begin{aligned} \widetilde{e}(Q,s) &= -se(Q,s) + 2Qh(Q,s), \\ \widetilde{h}(Q,s) &= -(Q/2)e(Q,s) + sh(Q,s), \end{aligned} \tag{3.64}$$

which obey

$$\begin{aligned}\phi_3(\sigma)\widetilde{e}(Q,s) &= -\frac{Q}{1-s}\mathbf{I}_3 + \mathcal{E}(Q,s),\\ \phi_4(\sigma)\widetilde{h}(Q,s) &= -\frac{s}{1-s}\mathbf{I}_3 + \mathcal{H}(Q,s).\end{aligned} \tag{3.65}$$

The solution of these equations is fully similar to that of equation (3.59). We are thus left with

$$\gamma_{33}(Q) = -\frac{3}{4}\frac{\mathcal{N}_{33}(Q)}{(1-Q^2)^2\left(H_3^2(Q,-Q)+H_4^2(Q,-Q)\right)}, \tag{3.66}$$

and with

$$\begin{aligned}\mathcal{N}_{33}(Q) &= Q^2(1+Q)^2H_4^2(Q,-Q)H_3^2(Q,-1) + Q^2(1-Q)^2H_3^2(Q,-Q)H_3^2(Q,-1)\\ &\quad +(1-Q)^2H_4^2(Q,-Q)H_4^2(Q,-1) + (1+Q)^2H_3^2(Q,-Q)H_4^2(Q,-1)\\ &\quad -8Q^2H_3(Q,-Q)H_4(Q,-Q)H_3(Q,-1)H_4(Q,-1).\end{aligned} \tag{3.67}$$

3.2.4. Derivation of $\gamma_{11}(Q)$, $\gamma_{12}(Q)$, and $\gamma_{22}(Q)$. — The determinant of the 4×4 linear system (3.47a), after a Laplace transformation, can be factorized as $(81/256)\phi_1(\sigma)\phi_2(\sigma)\phi_3(\sigma)\phi_4(\sigma)$. Its exact solution, along the lines of the previous cases, involves algebraic manipulations on very lengthy expressions. Some of them have been either carried out, or just checked, by means of the MACSYMA software. Furthermore, the final step of this calculation, involving the solution of the 9×9 linear system (3.74), must for practical purposes be performed numerically.

In a first step, the system (3.47a) is put in diagonal form by introducing the linear combinations

$$\begin{aligned}\widetilde{a}(Q,s) &= 2\sigma^2a(Q,s) - Q^2b(Q,s) - 2Qsd(Q,s) + 2Q^2g(Q,s),\\ \widetilde{b}(Q,s) &= -2\sigma^4a(Q,s) + (-2\sigma^4 - 2Q^2\sigma^2 + 2\sigma^2 + 3Q^2)b(Q,s)\\ &\quad +2Qs(-2\sigma^2+3)d(Q,s) + 2Q^2(2\sigma^2-3)g(Q,s),\\ \widetilde{d}(Q,s) &= Qsb(Q,s) + (\sigma^2+2Q^2)d(Q,s) - 2Qsg(Q,s),\\ \widetilde{g}(Q,s) &= (Q^2/2)b(Q,s) + Qsd(Q,s) - (2\sigma^2+Q^2)g(Q,s).\end{aligned} \tag{3.68}$$

These new functions obey

$$\begin{aligned}\phi_1(\sigma)\widetilde{a}(Q,s) &= \frac{2(s^2-1)(\mathbf{I}_1+\mathbf{I}_2) - 2Q^2\mathbf{I}_2}{1-s} + \widetilde{\mathcal{A}}(Q,s),\\ \phi_2(\sigma)\widetilde{b}(Q,s) &= \frac{2Q^2\mathbf{I}_1}{1-s} + \widetilde{\mathcal{B}}(Q,s),\\ \phi_3(\sigma)\widetilde{d}(Q,s) &= \frac{2Qs\mathbf{I}_1}{1-s} + \widetilde{\mathcal{D}}(Q,s),\\ \phi_4(\sigma)\widetilde{g}(Q,s) &= \frac{2s^2(\mathbf{I}_1-\mathbf{I}_2) + 2Q^2\mathbf{I}_2}{1-s} + \widetilde{\mathcal{G}}(Q,s),\end{aligned} \tag{3.69}$$

where $\widetilde{\mathcal{A}}(Q,s)$, $\widetilde{\mathcal{B}}(Q,s)$, $\widetilde{\mathcal{D}}(Q,s)$, and $\widetilde{\mathcal{G}}(Q,s)$ are defined in analogy with equation (3.20).

The formulae inverse to equation (3.68) read

$$\begin{aligned}4\sigma^4(\sigma^2-1)a(Q,s) &= \sigma^2(2\sigma^2+Q^2-2)\widetilde{a}(Q,s) + Q^2\widetilde{b}(Q,s)\\ &\quad +4Qs(\sigma^2-1)\widetilde{d}(Q,s) - 2Q^2(\sigma^2-1)\widetilde{g}(Q,s),\end{aligned}$$

$$
\begin{aligned}
4\sigma^4(\sigma^2-1)b(Q,s) &= -\sigma^2(2\sigma^2+3Q^2)\widetilde{a}(Q,s)-(2\sigma^2+3Q^2)\widetilde{b}(Q,s)\\
&\quad -12Qs(\sigma^2-1)\widetilde{d}(Q,s)+6Q^2(\sigma^2-1)\widetilde{g}(Q,s),\\
2\sigma^4(\sigma^2-1)d(Q,s) &= Qs\sigma^2\widetilde{a}(Q,s)+Qs\widetilde{b}(Q,s)\\
&\quad +2(\sigma^2-1)(\sigma^2+2Q^2)\widetilde{d}(Q,s)-2Qs(\sigma^2-1)\widetilde{g}(Q,s),\\
8\sigma^4(\sigma^2-1)g(Q,s) &= Q^2\sigma^2\widetilde{a}(Q,s)+Q^2\widetilde{b}(Q,s)\\
&\quad +4Qs(\sigma^2-1)\widetilde{d}(Q,s)-2(\sigma^2-1)(2\sigma^2+Q^2)\widetilde{g}(Q,s),
\end{aligned}
\tag{3.70}
$$

so that we have

$$
\begin{aligned}
\gamma_{11}(Q)\mathbf{I}_1+\gamma_{12}(Q)\mathbf{I}_2 &= -\frac{\widetilde{b}(Q,-1)+4Q\widetilde{d}(Q,-1)+2\widetilde{g}(Q,-1)}{2(1-Q^2)^2},\\
\gamma_{21}(Q)\mathbf{I}_1+\gamma_{22}(Q)\mathbf{I}_2 &= \frac{\widetilde{a}(Q,-1)+2\widetilde{g}(Q,-1)}{2(1-Q^2)}
\end{aligned}
\tag{3.71}
$$

The solution to equation (3.69) reads

$$
\begin{aligned}
\widetilde{a}(Q,s) &= \left(a_1+a_2s+\frac{a_3}{1-s}\right)H_1(Q,s),\\
\widetilde{b}(Q,s) &= \left(b_1+b_2s+b_3s^2+\frac{b_4}{1-s}\right)H_2(Q,s),\\
\widetilde{d}(Q,s) &= \left(d_1+d_2s+\frac{d_3}{1-s}\right)H_3(Q,s),\\
\widetilde{g}(Q,s) &= \left(g_1+g_2s+\frac{g_3}{1-s}\right)H_4(Q,s),
\end{aligned}
\tag{3.72}
$$

where $a_1, \cdot \quad , g_3$ are 13 Q-dependent constants to be determined.

The $s \to 1$ limit of equation (3.69) fixes four of these constants:

$$
\begin{aligned}
a_3 &= -\frac{3}{2}Q^2\mathbf{I}_2H_1(Q,-1), \quad b_4 = -3Q^2\mathbf{I}_1H_2(Q,-1),\\
d_3 &= -\frac{3}{2}Q\mathbf{I}_1H_3(Q,-1), \quad g_3 = -\frac{3}{4}\big(\mathbf{I}_1+(Q^2-1)\mathbf{I}_2\big)H_4(Q,-1).
\end{aligned}
\tag{3.73}
$$

The last nine constants are then determined by expressing that the functions $a(Q,s)$, , $g(Q,s)$ have the expected regularity properties at the points where the inversion formulas (3.70) are singular, namely $\sigma^2=0$, *i.e.*, $s=\pm Q$, or $\sigma^2=1$, *i.e.*, $s=\pm\sqrt{1+Q^2}$. We thus obtain the following system of nine linear equations

$$\widetilde{a}\left(Q,-\sqrt{1+Q^2}\right)+\widetilde{b}\left(Q,-\sqrt{1+Q^2}\right)=0, \tag{3.74a}$$

$$\widetilde{a}\left(Q,\sqrt{1+Q^2}\right)+\widetilde{b}\left(Q,\sqrt{1+Q^2}\right)=0, \tag{3.74b}$$

$$\widetilde{a}(Q,-Q)+2\widetilde{g}(Q,-Q)=0, \tag{3.74c}$$

$$\widetilde{b}(Q,-Q)-6\widetilde{g}(Q,-Q)=0, \tag{3.74d}$$

$$\widetilde{d}(Q,-Q)+2\widetilde{g}(Q,-Q)=0, \tag{3.74e}$$

$$\frac{\mathrm{d}}{\mathrm{d}s}\Big(\widetilde{b}(Q,s)+4\widetilde{d}(Q,s)+2\widetilde{g}(Q,s)\Big)_{s=-Q}-8Q\widetilde{g}(Q,-Q)=0, \tag{3.74f}$$

$$\widetilde{b}(Q,Q)-6\widetilde{g}(Q,Q)=0, \tag{3.74g}$$

$$\widetilde{d}(Q,Q) - 2\widetilde{g}(Q,Q) = 0, \tag{3.74h}$$

$$3\frac{\mathrm{d}}{\mathrm{d}s}\Big(\widetilde{b}(Q,s) - 4\widetilde{d}(Q,s) + 2\widetilde{g}(Q,s)\Big)_{s=Q} + 10Q\widetilde{a}(Q,Q) + 44Q\widetilde{g}(Q,Q) = 0, \tag{3.74i}$$

where (a) and (b) express the regularity of the functions $a(Q,s), \cdot \quad, g(Q,s)$ (absence of pole) at $s = \pm\sqrt{1+Q^2}$; (c) to (f) express their regularity (absence of double and of simple pole) at $s = -Q$; (g) to (i) express the absence of double pole at $s = Q$, as well as the proportionality of the residues of the simple poles to the right null vector of the system (3.47a), $\mathbf{V} = (3 - 2Q^2, 3 + Q^2, 2Q^2, Q^2/2)$.

The last of the above properties implies that the four functions $A(\tau)$, $B(\tau)$, $D(\tau)$, and $G(\tau)$ fall off as $\exp(-Q\tau)$. The dimensionless extinction length in the diffusive sector thus reads $\ell(Q) = 1/Q$ in units of the mean free path ℓ, *i.e.*,

$$L(q) = \frac{\ell}{Q} = \frac{1}{q} \tag{3.75}$$

in physical units. This simple result holds for any value of the transverse wavevector q. Moreover, since it is a bulk property of the problem, it also holds in the presence of an index mismatch, just as the extinction lengths of the non-diffusive sectors for $Q = 0$, determined in Section 3.1.4.

By inserting the explicit forms (3.72) into the expressions (3.74), we obtain a 9×9 linear system for the Q-dependent constants $\{a_1, a_2, b_1, b_2, b_3, d_1, d_2, g_1, g_2\}$, whose coefficients have complicated expressions involving the functions $H_n(Q,s)$. This system has been solved formally by means of the MACSYMA software: the outcome for each constant contains thousands of products of up to seven H-functions, so that this approach is of no practical use. The above system is however easily solved numerically, for any given value of Q. This is the way we have chosen to follow for practical purposes.

3.2.5. Summary of Results. — We have achieved the exact analytical determination of the enhanced backscattering cone in the absence of internal reflections. Its dependence on polarizations is contained in five functions of the reduced wavevector Q. Two of them, $\gamma_{33}(Q)$ and $\gamma_{44}(Q)$, are given explicitly in equations (3.62, 3.66), while the other three, $\gamma_{11}(Q)$, $\gamma_{12}(Q)$, and $\gamma_{22}(Q)$, are determined analytically, up to a last step which consists in solving numerically a well-posed 9×9 linear system, for any fixed value of Q.

The following regimes are of special interest.

• For small Q, *i.e.*, in the vicinity of the top of the cone, $\gamma_{11}(Q)$, $\gamma_{12}(Q)$, and $\gamma_{22}(Q)$ have the common characteristic triangular shape given by the general result (2.58), while $\gamma_{33}(Q)$ and $\gamma_{44}(Q)$ have a smooth dependence on Q^2. The enhancement factors and widths of the triangular cone, for linear and circular polarizations, have already been given in equations (3.41–3.44).

• For large Q, *i.e.*, in the wings of the cone, the leading contributions come from low-order scattering events, as usual. The single-scattering contribution (2.45) is of little interest, since it is subtracted in the formula (2.41) for the enhanced backscattering peak. The leading large-Q behaviour of the enhancement factor is thus given by double-scattering events. The contribution of this class of events can be obtained by solving equation (3.47) to first order in the kernels M_{pq}. As it turns out, for large Q these kernels become small, as expected, but also local in the τ-variable: $M_{pq}(\tau,\tau') \approx m_{pq}(Q,0)\delta(\tau - \tau')$. Furthermore, only the following kernels contribute to leading order in $1/Q$:

$$m_{00} \approx \frac{\pi}{2Q}, \quad m_{02} \approx \frac{\pi}{4Q}, \quad m_{04} \approx \frac{3\pi}{16Q}, \quad m_{20} \approx \frac{\pi}{4Q}, \quad m_{22} \approx \frac{\pi}{16Q}, \quad m_{40} \approx \frac{3\pi}{16Q}, \tag{3.76}$$

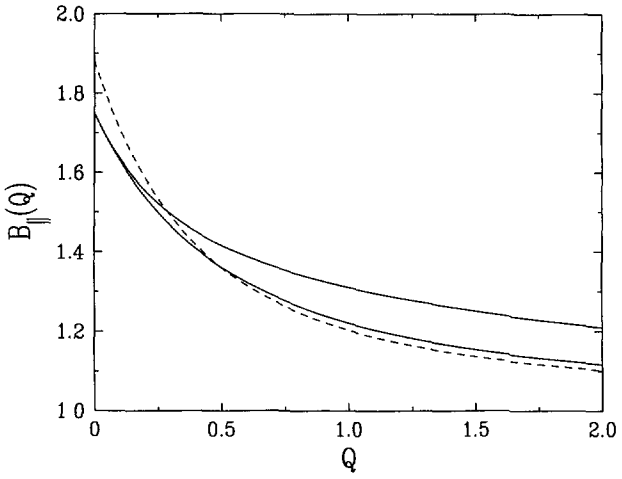

Fig. 3. — Plot of enhancement factors $B_{\parallel}(Q)$ for linearly polarized beams at normal incidence and parallel detection, in the absence of internal reflections, in two cases defined in the text. Upper full line: case (i) ($\psi_a = \psi_b = 0$). Lower full line: case (ii) ($\psi_a = \psi_b = \pi/2$). Dashed line: same quantity for isotropic scattering of scalar waves, from reference [19].

so that we are left with

$$\gamma_{11}(Q) \approx \frac{3}{4}\left(1+\frac{3\pi}{4Q}\right), \quad \gamma_{22}(Q) \approx \frac{3}{4}\left(1+\frac{9\pi}{32Q}\right), \quad \gamma_{33}(Q) \approx \gamma_{44}(Q) \approx -\frac{3}{4}\left(1+\frac{3\pi}{8Q}\right). \tag{3.77}$$

We end up by illustrating a few interesting features of our results. We first consider linearly polarized beams at normal incidence and for parallel detection, in the following two geometries:
(i) both polarizations parallel to **Q**, *i.e.*, $\psi_a = \psi_b = 0$,
(ii) both polarizations perpendicular to **Q**, *i.e.*, $\psi_a = \psi_b = \pi/2$.
The enhancement factors, given by equation (2.53), namely

$$B_{\parallel}^{(\mathrm{i})}(Q) = 1 + \frac{\gamma_{11}(Q) - 3/4}{\gamma_{11}(0)}, \quad B_{\parallel}^{(\mathrm{ii})}(Q) = 1 + \frac{\gamma_{22}(Q) - 3/4}{\gamma_{11}(0)}, \tag{3.78}$$

are plotted in Figure 3. Both curves coincide with the result (3.41) at $Q = 0$, while they are slightly different from each other at $Q \neq 0$. The enhancement factor of isotropic scattering of scalar waves, from references [19,30], is also shown for comparison.

Similarly, we consider linearly polarized beams with perpendicular detection, in the following two cases:
(iii) one polarization parallel to **Q**, *i.e.*, $\psi_a = 0$, $\psi_b = \pi/2$,
(iv) both polarizations at 45° with respect to **Q**, *i.e.*, $\psi_a = -\psi_b = \pi/4$.
The enhancement factors,

$$B_{\perp}^{(\mathrm{iii})}(Q) = 1 + \frac{\gamma_{44}(Q) - \gamma_{33}(Q)}{2\gamma_{12}(0)}, \quad B_{\perp}^{(\mathrm{iv})}(Q) = 1 + \frac{\gamma_{11}(Q) + \gamma_{22}(Q) - 2\gamma_{12}(Q) + 2\gamma_{44}(Q)}{4\gamma_{12}(0)}, \tag{3.79}$$

are plotted in Figure 4. Both factors coincide with the result (3.41) at $Q = 0$, while they are slightly different from each other at $Q \neq 0$.

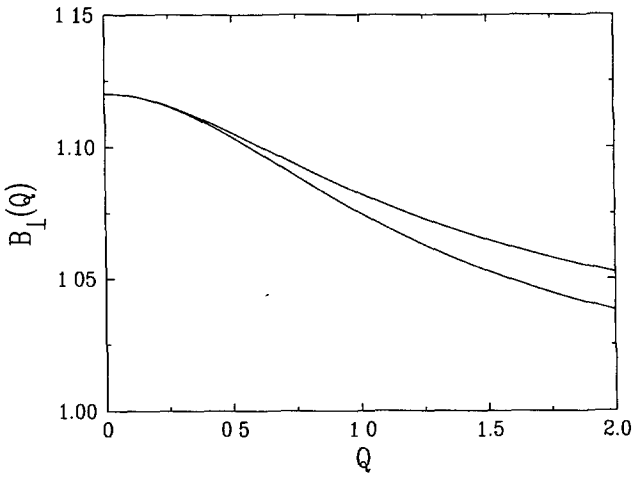

Fig. 4. — Plot of enhancement factors $B_{\perp}(Q)$ for linearly polarized beams at normal incidence and perpendicular detection, in the absence of internal reflections, in two cases defined in the text. Lower full line: case (iii) ($\psi_a = 0$, $\psi_b = \pi/2$). Upper full line: case (iv) ($\psi_a = -\psi_b = \pi/4$).

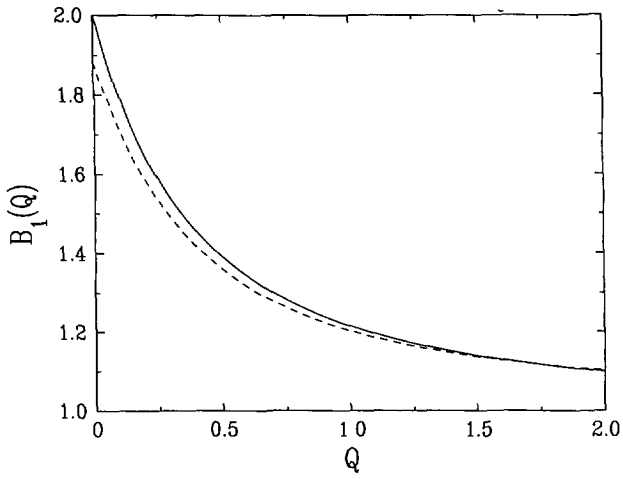

Fig. 5. — Plot (full line) of enhancement factor $B_1(Q)$ for circularly polarized beams at normal incidence in the helicity-preserving channel, in the absence of internal reflections. Dashed line: same quantity for isotropic scattering of scalar waves, from reference [19].

We end up by considering circularly polarized beams at normal incidence. The enhancement factors $B_1(Q)$ of the helicity-preserving channel, and $B_{-1}(Q)$ of the channel of opposite helicity, given by inserting the above results into the general expressions (2.54), (2.63), are plotted in Figures 5 and 6, respectively.

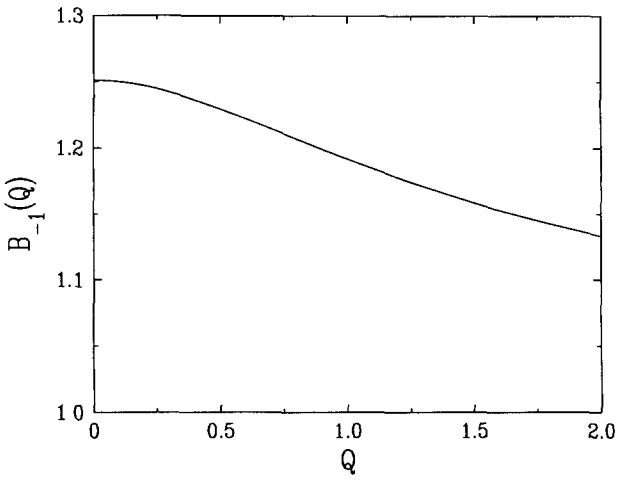

Fig. 6. — Plot of enhancement factor $B_{-1}(Q)$ for circularly polarized beams at normal incidence in the channel of opposite helicity, in the absence of internal reflections.

4. Large Index Mismatch Regime

Previous works [19–21] on multiple scattering of scalar waves suggest that the SM equations cannot be solved analytically in the presence of internal reflections, which take place whenever the index mismatch $m = n/n_1$ is different from unity. However, and interestingly enough, it has been shown in references [19–21] that the problem becomes again tractable by analytical means in the regime of a large index mismatch ($m \ll 1$ or $m \gg 1$), at least in the case of scalar waves. The intuitive origin of this simplification is as follows. If the ratio m of both optical indices is very small (respectively, very large), there is total reflection for almost any incidence angle outside the medium (respectively, inside the medium), except for a narrow cone around the normal incidence. As a consequence, the radiation undergoes many internal reflections at the boundary of the sample, and hence many scattering events, before it can exit the medium. In this section we extend this approach to the Rayleigh scattering of electromagnetic waves.

4.1. Diffuse Reflection and Transmission. — In this section we investigate the diffuse intensity in reflection and in transmission in the large index mismatch regime. To do so, it is advantageous to consider the matrix Green's function $\mathbf{G}(\tau, \mu, \varphi, \tau', \mu', \varphi')$, which obeys equation (2.13). We anticipate on physical grounds that only the φ-independent sector ($k = 0$) is important. We thus rewrite equation (2.13) as

$$\begin{aligned}
\mathbf{G}^{(0)}(\tau, \mu, \tau', \mu') &= \mathbf{P}^{(0)}(\mu, \mu')\delta(\tau - \tau') \\
&+ \int_0^{\tau} \mathrm{d}\tau'' \int_0^1 \frac{\mathrm{d}\mu''}{2\mu''} \mathrm{e}^{-(\tau-\tau'')/\mu''} \mathbf{P}^{(0)}(\mu, \mu'') \cdot \mathbf{G}^{(0)}(\tau'', \mu'', \tau', \mu') \\
&+ \int_{\tau}^{+\infty} \mathrm{d}\tau'' \int_0^1 \frac{\mathrm{d}\mu''}{2\mu''} \mathrm{e}^{-(\tau''-\tau)/\mu''} \mathbf{P}^{(0)}(\mu, -\mu'') \cdot \mathbf{G}^{(0)}(\tau'', -\mu'', \tau', \mu') \\
&+ \int_0^{+\infty} \mathrm{d}\tau'' \int_0^1 \frac{\mathrm{d}\mu''}{2\mu''} \mathrm{e}^{-(\tau+\tau'')/\mu''} \mathbf{P}^{(0)}(\mu, \mu'') \cdot \mathbf{G}^{(0)}(\tau'', \mu'', \tau', \mu') \\
&- \int_0^{+\infty} \mathrm{d}\tau'' \int_0^1 \frac{\mathrm{d}\mu''}{2\mu''} \mathrm{e}^{-(\tau+\tau'')/\mu''} \big(\mathbf{1} - \mathbf{R}(\mu'')\big) \cdot \mathbf{P}^{(0)}(\mu, \mu'') \cdot \mathbf{G}^{(0)}(\tau'', \mu'', \tau', \mu'). \qquad (4.1)
\end{aligned}$$

The above observations suggest to treat the small matrix $\mathbf{1} - \mathbf{R}(\mu)$ as a perturbation. In the limit of an infinite index mismatch ($m = 0$ or $m = +\infty$), this matrix vanishes identically. The rest of equation (4.1), without the last line, has a zero mode of the form

$$\mathbf{M}_{\rm nat} = \mathbf{I}_{\rm nat} \otimes \mathbf{I}_{\rm nat} = \begin{pmatrix} 1 & 1 & 0 & 0 \\ 1 & 1 & 0 & 0 \\ 0 & 0 & 0 & 0 \\ 0 & 0 & 0 & 0 \end{pmatrix}, \tag{4.2}$$

independent of τ and μ. This is demonstrated by the identity

$$\int_{-1}^{1} \frac{\mathrm{d}\mu}{2} \mathbf{M}_{\rm nat} \cdot \mathbf{P}^{(0)}(\mu, \mu') = \mathbf{M}_{\rm nat} \quad \text{for all } \mu'. \tag{4.3}$$

Along the lines of references [19–21], we expect that the Green's function becomes proportional to the constant matrix $\mathbf{M}_{\rm nat}$, with a diverging prefactor, in the large index mismatch regime. We thus look for a singular expansion of the form

$$\mathbf{G}^{(0)}(\tau, \mu, \tau', \mu') = C\mathbf{M}_{\rm nat} + \mathbf{G}_0^{(0)}(\tau, \mu, \tau', \mu') + \cdot \quad , \tag{4.4}$$

where it is understood that the constant C diverges as $m \to 0$ or $m \to +\infty$, while $\mathbf{G}_0^{(0)}$ stays finite, and the dots stand for higher-order corrections. We insert this expansion into equation (4.1), and then act on both sides with the operator $\int_0^{+\infty} \mathrm{d}\tau \int_{-1}^{1} (\mathrm{d}\mu/2) \mathbf{M}_{\rm nat}$. Integrals over the finite part $\mathbf{G}_0^{(0)}$ of the Green's function cancel out, so that we are left with a simple expression for the constant C, namely

$$C = \frac{2}{\mathcal{T}}, \tag{4.5}$$

with

$$\mathcal{T} = \frac{\mathcal{T}_\parallel + \mathcal{T}_\perp}{2}, \quad \mathcal{T}_\parallel = \int_0^1 2\mu \mathrm{d}\mu \, T_\parallel(\mu), \quad \mathcal{T}_\perp = \int_0^1 2\mu \mathrm{d}\mu \, T_\perp(\mu). \tag{4.6}$$

The above quantities only depend on the index mismatch m. They are interpreted as the mean flux transmission coefficients of one boundary of the sample, averaged over incidence angles. $\mathcal{T}_\parallel$ and $\mathcal{T}_\perp$ correspond to prescribed polarizations, while $\mathcal{T}$ is also averaged over both polarization channels.

More explicitly, the expressions (2.8, 2.9) of the Fresnel intensity coefficients allow us to perform the integrals (4.6) in closed form, for both $m \geq 1$ and $m \leq 1$. It turns out that both cases can be gathered in the following formulas, valid for $m \geq 1$:

$$\begin{aligned} m\mathcal{T}_\perp(m) = \frac{1}{m}\mathcal{T}_\perp\left(\frac{1}{m}\right) &= \frac{4(2m+1)}{3m(m+1)^2}, \\ m\mathcal{T}_\parallel(m) = \frac{1}{m}\mathcal{T}_\parallel\left(\frac{1}{m}\right) &= \frac{2m(m^2-1)^2}{(m^2+1)^3} \ln\frac{m+1}{m-1} \\ &\quad - \frac{16m^3(m^4+1)}{(m^2-1)^2(m^2+1)^3} \ln m + \frac{4m^2(m^2+2m-1)}{(m^2-1)(m^2+1)^2}. \end{aligned} \tag{4.7}$$

As expected, the flux transmission coefficients vanish in the regime of a large index mismatch, according to

$$\begin{aligned} m \to 0: &\quad \mathcal{T}_\parallel \approx 8m, \quad \mathcal{T}_\perp \approx \frac{8m}{3}, \quad \mathcal{T} \approx \frac{16m}{3}, \\ m \to +\infty: &\quad \mathcal{T}_\parallel \approx \frac{8}{m^3}, \quad \mathcal{T}_\perp \approx \frac{8}{3m^3}, \quad \mathcal{T} \approx \frac{16}{3m^3}. \end{aligned} \tag{4.8}$$

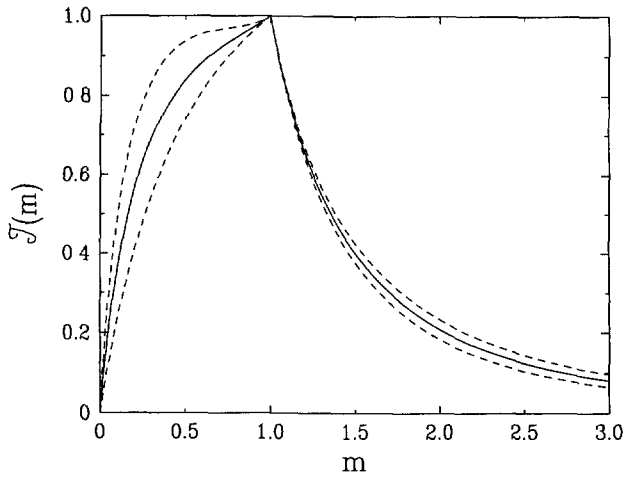

Fig. 7. — Plot of mean flux transmission coefficients, against optical index mismatch m. Upper dashed line: $\mathcal{T}_{\|}(m)$. Lower dashed line: $\mathcal{T}_{\perp}(m)$ (also corresponds to scalar waves). Full line: their average $\mathcal{T}(m)$.

The knowledge of the matrix Green's function yields by equations (2.16, 2.22–2.24) the following predictions for observables of interest in the large index mismatch regime

$$\begin{aligned} \gamma_{ij}^{(0)}(\mu_a, \mu_b) &\approx \frac{2\mu_a\mu_b}{\mathcal{T}} \quad (i,j=1,2), \\ \tau_i(\mu) &\approx \frac{2\mu}{\mathcal{T}} \quad (i=1,2), \\ \tau_0 &\approx \frac{4}{3\mathcal{T}}. \end{aligned} \tag{4.9}$$

These leading-order results in the large index mismatch regime are very similar to those obtained in the case of isotropic [19,20] and arbitrary anisotropic [21] scattering of scalar waves. Figure 7 shows plots of the mean transmission amplitudes $\mathcal{T}$, $\mathcal{T}_{\|}$, and $\mathcal{T}_{\perp}$, against the index mismatch m. It is worth noticing that the reflection and transmission coefficients for scalar waves coincide with $R_{\perp}(\mu)$ and $T_{\perp}(\mu)$, so that $\mathcal{T}_{\perp}$ was already involved in the predictions of references [19–21] for scalar waves.

The behaviour of the quantities investigated above in the large index mismatch regime involves, besides the leading asymptotic behaviour in $1/\mathcal{T}$ derived above, finite parts related to the Green's function $\mathbf{G}_0^{(0)}$ Moreover, $\mathbf{G}_0^{(0)}$ also governs the (non-divergent) large index mismatch behaviour of all the other quantities, like *e.g.* the entries of the bistatic matrix $\gamma_{ij}^{(0)}$ outside the (1, 2) sector, or the bistatic matrices $\gamma_{ij}^{(k)}$ for $k \neq 0$. These finite parts cannot be determined analytically in general. In the case of isotropic scattering of scalar waves, the finite parts of some simple observables have been determined [19, 20], either analytically or numerically.

4.2. Enhanced Backscattering Cone. — We now extend the above analysis to the enhanced backscattering cone. In analogy with the case of scalar waves, treated in references [19–21], we want to show that the bistatic matrix $\gamma(Q)$ takes a simple scaling form in

the regime of small Q and large index mismatch, where enhanced backscattering is dominated by long-distance effects.

To do so, we look for a solution to the Q-dependent SM equations (2.46) in the form

$$\mathbf{\Gamma}^{(k)}(\tau,\mu) \approx a(Q)\mathrm{e}^{-Q\tau}\mathbf{M}_{\mathrm{nat}}\delta_{k0}, \tag{4.10}$$

for $m \ll 1$ or $m \gg 1$, and $Q \ll 1$. The above ansatz is justified as follows: the exponential fall-off in $\exp(-Q\tau)$ is quite general (see Eq. (3.75)); the φ-dependent sectors ($k \neq 0$) are again neglected; the proportionality to the matrix $\mathbf{M}_{\mathrm{nat}}$ is assumed because of the structure (4.2, 4.3) of the zero mode of the RTT problem at $Q = 0$.

In analogy with Section 4.1, we insert the form (4.10) into equation (2.46), and then act on both sides with the operator $\int_0^{+\infty} \mathrm{d}\tau \int_{-1}^{1} (\mathrm{d}\mu/2)\mathbf{M}_{\mathrm{nat}}$. The integrals which do not involve the small matrix $\mathbf{1} - \mathbf{R}(\mu)$ can be performed exactly; their Q-dependence is given by $m_{00}(Q,0) = m_0(iQ) = \arctan(Q)/Q \approx 1 - Q^2/3$, by equation (3.7). The Q-dependence of the integral involving $\mathbf{1} - \mathbf{R}(\mu)$ can be neglected. Consistently neglecting all corrections of order Q^2, we obtain

$$\gamma_{ij}(Q) \approx \frac{1}{\dfrac{2Q}{3} + \dfrac{\mathcal{T}}{2}} \quad (i,j = 1,2). \tag{4.11}$$

This prediction of the leading behaviour of the enhanced backscattering cone in the large index mismatch regime is again very similar to the case of scalar waves [19–21].

We end up by giving a few consequences of the above predictions in the large index mismatch regime. In the case of linear polarizations, the enhancement factor (2.55) at the top of the cone reads $B(0) = 2\cos^2\Psi$. It assumes the maximal value $B_{\parallel} = 2$ for parallel detection, because the single-scattering contribution is negligible. The width of the top of the cone (2.61) reads

$$\Delta Q_{\parallel} \approx \frac{3\mathcal{T}}{4}. \tag{4.12}$$

This last result also gives the width ΔQ_1 of the top of the cone of enhanced backscattering for the helicity-preserving channel (2.66) in the case of circular polarizations.

5. Discussion

In this paper we have extended to the Rayleigh scattering of electromagnetic waves our previous investigations [19–21] of multiple scattering of scalar waves in a thick-slab geometry. Both the setup and the formalism of the present work closely follow those references, so that only the main lines of the derivations have been reproduced here. The main advantage of this approach, based on RTT, is that the role of skin layers, and especially the effects of internal reflections, are incorporated in a natural way. The present approach has no phenomenological or approximate character, besides the restriction of its validity to the regime $\lambda \ll \ell \ll L$, in contrast with the widely used diffusion approximation. Only few analytical results [17, 18] had been obtained for electromagnetic waves along this line of thought, since the pioneering work of Chandrasekhar [1]. It is, however, worth mentioning that the vector RTT formalism, including the effects of internal reflections, has been exposed earlier [31, 32], although these authors only solved the SM equations numerically in some specific situations, rather than investigating their general properties. We have first derived general results on vector RTT in Section 2, where the mean values of observables are expressed in terms of solutions to vector SM equations, including the effects of polarizations and of internal reflections. Closed-form

expressions for these general predictions are then derived in two cases, namely in the absence of internal reflections (in Sect. 3), and in the regime of a large index mismatch (in Sect. 4).

In the absence of internal reflections ($m = n/n_1 = 1$), the SM equations have been solved by means of the Wiener-Hopf technique. We have presented in Section 3 a self-contained exposition of all the exact results known so far [1]. More importantly, we have given the first complete analytical derivation of the cone of enhanced backscattering, completing thus the analytical results of references [17,18], as well as some less accurate estimates, obtained either by means of the diffusion approximation or by numerical simulations [10,11,13]. As a general rule, illustrated by the first three items of Table II, quantities which are either averaged over the polarization degrees of freedom, or do not depend on polarizations at all, are found to be very close to the corresponding figures in the case of multiple isotropic scattering of scalar waves. A similar observation has been made in reference [21], where various observables were compared for isotropic and very anisotropic (forward) scattering of scalar waves. The prototype of such quantities is the thickness τ_0 of a skin layer, expressed in units of the transport mean free path ℓ^*. This number is hardly sensitive to the anisotropy of the scattering mechanism nor to polarizations: it always comes out to read $\tau_0 \approx 0.71$ [4].

Other observables, such as the detailed shape of the cone of enhanced backscattering, have a more or less pronounced dependence on the polarization channels of the incident and detected beams. The last two items of Table II illustrate this point. The first quantity under consideration is the maximal enhancement factor, right at the top of the cone. The value $B_{\|}$ of equation (3.41), corresponding to linear polarizations and parallel detection, as well as the value B_1 of equation (3.43), corresponding to circular polarizations and detection in the channel of same helicity, are compared to the analogous result for scalar waves with isotropic scattering [19,30], denoted by B: the figures are definitely different from each other, although relatives differences are less than 10%. Second, the width of the triangular top of the backscattering cone is considered. The value $\Delta Q_{\|}$ of equation (3.42), corresponding to linear polarizations and parallel detection, as well as the value ΔQ_1 of equation (3.44), corresponding to circular polarizations and detection in the channel of same helicity, are compared to the analogous result for scalar waves with isotropic scattering [19, 30], denoted by ΔQ: relative differences are more important in this case, going up to some 40%. Finally, so far there are essentially no analytical results concerning the RTT approach to the general problem of multiple scattering of electromagnetic waves, taking into account the combined effects of anisotropic scattering and polarizations. We can infer from the results of reference [21] on the multiple scattering of scalar waves that the anisotropy of the scattering mechanism will have little residual effects, once the principal scaling is taken into account by expressing observables in terms of the transport mean free path ℓ^*.

In the presence of internal reflections ($m = n/n_1 \neq 1$), analytical predictions for the various observables of interest have been derived in the large index mismatch regime ($m \ll 1$ or $m \gg 1$), along the lines of previous investigations of scalar waves, with isotropic [19,20] and arbitrary anisotropic [21] scattering. The effects of internal reflections have been studied [22–25] using several variants of the diffusion approximation. Reference [26] provides a recent overview of these approaches to the subject. Within the framework of RTT, the drastic simplification which takes place in the large index mismatch regime has a clear intuitive explanation. Since the transmission through the boundaries of the sample is small, radiation is reinjected many times before it can leave the medium. As a consequence, the skin layers become very thick and, more importantly, the radiation field is uniform over most of these layers. The results (4.9) turn out to have the very same form as for multiple scattering of scalar waves, either with isotropic [19, 20] or very anisotropic [21] scattering. Most certainly, the very same analytical forms also hold true in the more general case of multiple scattering of electromagnetic waves,

including both anisotropy and polarization effects, and they are expected to provide an overall satisfactory description of the full dependence of physical quantities on the index mismatch, especially in the range of most interest ($m \geq 1$).

The present investigations of multiple Rayleigh scattering of electromagnetic waves, as well as the previous ones on isotropic and anisotropic scattering of scalar waves [19–21], have so far only dealt with the mean intensity, averaged over the random positions of the scatterers in the sample. For any given sample of scattering medium, however, the intensity has strong fluctuations, which manifest themselves as speckles. For instance, the probability law of the fluctuating intensity at a given point is known as Rayleigh's law: $p(I) \sim \exp(-I/\langle I \rangle)$. The generalization of Rayleigh's law to polarized radiation is fully characterized by the four Stokes parameters [33]. Various correlation functions, aiming at a more detailed description of intensity fluctuations and speckle patterns, have been the subject of recent theoretical and experimental investigations [34]. We mention the extension of these results, in order to include polarization effects, as an interesting open problem.

Acknowledgments

The work of Th.M.N. has been supported by the Royal Dutch Academy of Arts and Sciences (KNAW).

References

[1] Chandrasekhar S., Radiative Transfer (Dover, New-York, 1960).
[2] Sobolev V.V., A Treatise on Radiative Transfer (Van Nostrand, Princeton, N.J., 1963).
[3] Ishimaru A., Wave Propagation and Scattering in Random Media, in 2 volumes (Academic, New-York, 1978).
[4] van de Hulst H.C., Multiple Light Scattering, in 2 volumes (Academic, New-York, 1980).
[5] Kuga Y. and Ishimaru A., *J. Opt. Soc. Am. A* **1** (1984) 831; van Albada M.P. and Lagendijk A., *Phys. Rev. Lett.* **55** (1985) 2692; Wolf P.E. and Maret G., *Phys. Rev. Lett.* **55** (1985) 2696.
[6] van der Mark M.B., van Albada M.P. and Lagendijk A., *Phys. Rev. B* **37** (1988) 3575.
[7] Ishimaru A. and Tsang L., *J. Opt. Soc. Am. A* **5** (1988) 228.
[8] Papanicolaou G.C. and Burridge R., *J. Math. Phys.* **16** (1975) 2074.
[9] Watson K.M., *J. Math. Phys.* **10** (1969) 688.
[10] Stephen M.J. and Cwilich G., *Phys. Rev. B* **34** (1986) 7564; Cwilich G. and Stephen M.J., *Phys. Rev. B* **35** (1987) 6517.
[11] Akkermans E., Wolf P.E., Maynard R. and Maret G., *J. Phys. France* **49** (1988) 77.
[12] MacKintosh F.C. and John S., *Phys. Rev. B* **37** (1988) 1884; *Phys. Rev. B* **40** (1989) 2383.
[13] van Albada M.P. and Lagendijk A., *Phys. Rev. B* **36** (1987) 2353.
[14] van Tiggelen B.A., Maynard A. and Nieuwenhuizen Th.M., *Phys. Rev. B* **53** (1996) 2881.
[15] van Tiggelen B.A., *Phys. Rev. Lett.* **75** (1995) 422.
[16] Peters K.J., *Phys. Rev. B* **46** (1992) 801.
[17] Mishchenko M.I., *Phys. Rev. B* **44** (1991) 12597; *J. Opt. Soc. Am. A* **9** (1992) 978.
[18] Ozrin V.D., *Waves in Random Media* **2** (1992) 141.
[19] Nieuwenhuizen Th.M. and Luck J.M., *Phys. Rev. E* **48** (1993) 569.

[20] Nieuwenhuizen Th.M., Veelvoudige verstrooing van golven, unpublished lecture notes in Dutch (University of Amsterdam, 1993).
[21] Amic E., Luck J.M. and Nieuwenhuizen Th.M., *J. Phys. A* **29** (1996) 4915.
[22] Lagendijk A., Vreeker R. and de Vries P., *Phys. Lett. A* **136** (1989) 81.
[23] Freund I. and Berkovits R., *Phys. Rev. B* **41** (1990) 496.
[24] Zhu J.X., Pine D.J. and Weitz D.A., *Phys. Rev. A* **44** (1991) 3948.
[25] Freund I., *Phys. Rev. A* **45** (1992) 8854.
[26] Freund I., *J. Opt. Soc. Am. A* **11** (1994) 3274.
[27] Born M. and Wolf E., Principles of Optics (Pergamon, 1965).
[28] Wiersma D.S., van Albada M.P., van Tiggelen B.A. and Lagendijk A., *Phys. Rev. Lett.* **74** (1995) 4193.
[29] van Tiggelen B.A., Wiersma D.S. and Lagendijk A., *Europhys. Lett.* **30** (1995) 1.
[30] Gorodnichev E.E., Dudarev S.L. and Rogozkin D.B., *Phys. Lett. A* **144** (1990) 48.
[31] Tsang L. and Kong J.A., *Radio Sci.* **13** (1978) 763; Shin R.T. and Kong J.A., *J. Appl. Phys.* **52** (1981) 4221.
[32] Ma Q. and Ishimaru A., *IEEE Trans. Antennas and Propagation* **39** (1991)1626; Lam C.M. and Ishimaru A., *IEEE Trans. Antennas and Propagation* **41** (1993) 851.
[33] Mandel L., *Proc. Phys. Soc.* **81** (1963) 1104, and references therein.
[34] van Rossum M.C.W., de Boer J.F. and Nieuwenhuizen Th.M., *Phys. Rev. E* **52** (1995) 2053, and references therein.